ELSEVIER

Chemical Geology 220 (2005) 165–189

CHEMICAL GEOLOGY
INCLUDING
ISOTOPE GEOSCIENCE

www.elsevier.com/locate/chemgeo

Nature of the Mesozoic lithospheric mantle and tectonic decoupling beneath the Dabie Orogen, Central China: Evidence from $^{40}Ar/^{39}Ar$ geochronology, elemental and Sr–Nd–Pb isotopic compositions of early Cretaceous mafic igneous rocks

Yuejun Wang[a,*], Weiming Fan[a], Touping Peng[a], Hongfu Zhang[b], Feng Guo[a]

[a]*Key Laboratory of Isotope Geochronology and Geochemistry, Guangzhou Institute of Geochemistry, Chinese Academy of Sciences, P.O. Box 1131, Guangzhou 510640, China*

[b]*Institute of Geology and Geophysics, Chinese Academy of Sciences, Beijing 100029, China*

Received 9 December 2003; accepted 28 February 2005

Abstract

Geochronological, elemental and Sr–Nd–Pb isotopic data of early Cretaceous basic-intermediate rocks from the Dabie Orogen provide new insights into the nature of the late Mesozoic lithospheric mantle beneath the region and its tectonic relationship with neighboring blocks. Basic-intermediate rocks from the North Dabie Complex (NDC) include diabases, lamprophyres and trachyandesites, which have $^{40}Ar/^{39}Ar$ plateau ages of 127.6–131.8 Ma. Similar rock types from the North Huaiyang Unit (NHY) erupted at nearly the same time (135–116 Ma). Coeval rocks from both tectonic units form a continuous array in Harker diagrams, and exhibit similar geochemical characteristics. Both are significantly enriched in LILEs, and depleted in HFSEs, coupled with very low $\varepsilon_{Nd}(t)$, $(^{206}Pb/^{204}Pb)_i$, and prominent positive $\Delta 8/4$ and $\Delta 7/4$ values, which are similar to those of Mesozoic mafic rocks in the North China Craton (NCC) exterior. These geochemical signatures are inconsistent with crustal contamination during magma ascent, and reflect derivation from an enriched lithospheric mantle source contaminated by the deeply subducted Yangtze crust. The observed geochemical similarities thus suggest that early Cretaceous igneous rocks from the NDC and NHY share a similar continental lithospheric mantle source that is tectonically affiliated to the NCC, although the surface geology of both tectonic units correlates with that of the Yangtze Block. Tectonic decoupling along a suture is proposed to explain the generation of early Cretaceous mafic rocks in the Dabie Orogen. The Wuhe-Shuihou fault likely represents the Mesozoic lithospheric boundary between the Yangtze Block and NCC, despite the fact that the present-day surface suture is situated at the Xiaotian-Mozitan fault or other faults to the north.

Keywords: $^{40}Ar/^{39}Ar$ geochronology; Sr–Nd–Pb isotopes; Early Cretaceous basic-intermediate rocks; Continental lithospheric mantle; Tectonic decoupling; Dabie Orogen

* Corresponding author. Tel.: +86 20 85290527; fax: +86 20 85290708.
E-mail addresses: yjwang@gig.ac.cn, wangyj6@21cn.com (Y. Wang).

0009-2541/$ - see front matter © 2005 Elsevier B.V. All rights reserved.
doi:10.1016/j.chemgeo.2005.02.020

1. Introduction

The Dabie-Sulu high- and ultrahigh-pressure (HP-UHP) metamorphic belt was formed by Triassic northward subduction of the Yangtze Block (YB) and subsequent collision with the North China Craton (NCC) (e.g., Li et al., 1993; Cong, 1996). The Yangtze crustal materials were brought into mantle depths (e.g. Mattauer et al., 1985; Okay et al., 1993; Cong, 1996; Hacker et al., 1998; Ye et al., 2000; Fan et al., 2004) and then rapidly exhumed to middle/lower crustal levels at 230–210 Ma (Okay et al., 1993; Hacker et al., 1998; Zheng et al., 2003). The subduction-related fluid/melt might have migrated up and interacted with the surrounding mantle and caused metasomatism in the overlying lithospheric mantle (e.g., Zhang et al., 2002a,b). Alternatively the subducted crustal materials could have been partly trapped in the mantle to produce a hybridized source (Jahn et al., 1999; Fan et al., 2004). A series of studies on Cretaceous mafic/ultramafic intrusions (~125 Ma) from the Dabie Orogen, late Mesozoic volcanic rocks (150–116 Ma) from the North Huaiyang Unit (NHY), and basaltic rocks from the Fangcheng and Laiyang areas adjacent to or within the Sulu belt (Fig. 1a) show that these rocks have very low $\varepsilon_{Nd}(t)$ values (−22 to −14), suggesting derivation from an enriched lithospheric mantle modified by subduction process (Chen et al., 2002; Wang et al., 2002; Li and Yan, 2003; Zhang et al., 2002a,b; Fan et al., 2001). However, continued debates remain over the nature of the Mesozoic lithospheric mantle beneath the Dabie Orogen and the possibility that subducted materials were preserved at mantle depth as relicts. Furthermore, controversies also include: (1) the location of the suture beneath the Dabie Orogen (Ames et al., 1996; Rowley et al., 1997; Zhang et al., 1994, 2002a,b; Kuang and Zhang, 2002; Suo et al., 2000; Hacker et al., 1998, 2000; Cong, 1996; Li and Yan, 2003; Wang et al., 2003a), and (2) the tectonic affiliation of the North Dabie Complex Unit (NDC). Although tectonic decoupling of the present-day surface and subsurface sutures in the region east of the Tan-Lu fault was already suggested by Li (1994) and Chung (1999), questions particularly concerning the location of the lithospheric suture boundary and whether a crustal detachment also developed in the region west of the Tan-Lu Fault (Li and Yan, 2003) have not been appropriately addressed.

The YB and NCC have distinctive crustal ages and tectonic evolution histories (Cong, 1996; Qiu et al., 2000), and therefore they should have different lithospheric mantle sources that could be traced by mafic magmatism. In the Dabie Orogen, geochemical and Sr–Nd isotopic studies have mostly focused on Mesozoic mafic/ultramafic intrusions (Jahn et al., 1999; Li and Yan, 2003 and references therein) and granitoids (Ma et al., 1998, 2000; Chen et al., 2002; Zhang et al., 2002a,b). Recently Fan et al. (2004) reported the geochronology, and elemental and Sr–Nd isotopic compositions of early Cretaceous basaltic-andesitic rocks from the NHY, and concluded that these rocks were derived from an enriched lithospheric mantle with subducted continental crustal relicts. They further proposed that a significant volume of the subducted continental crust might be trapped in the original lithospheric mantle while some were rapidly exhumed to the crustal levels shortly after collision. Little attention, however, has been paid to the less abundant Mesozoic mafic dikes emplaced in the NDC (Chen et al., 1995). These rocks provide a possibility to constrain the nature of the mantle source beneath the NDC and to define the lithospheric boundary between the YB and NCC. Therefore, in this paper, we present a set of geochronological, elemental and Sr–Nd–Pb isotopic data of early Cretaceous mafic dikes from the NDC and Pb

Fig. 1. (a) Tectonic subdivision of the Dabie-Sulu orogenic belt (after Jahn et al., 1999). Black ellipses mark the distributions of major Mesozoic mafic rocks from the Dabie Orogen (NHY and NDC) and North China Craton (NCC) exterior derived from subduction-related lithospheric mantle (e.g., Fangcheng, Mengyin and Laiyang in Jiaodong). Early Cretaceous basaltic rocks from the Central NCC (i.e., Taihangshan, Jinan and Jiyang), Susong blueschist unit (i.e., Macheng) and northern Yangtze block (i.e., Huangshi-Xinzhou and lower Yangtze river region) are shown by grey ellipse and dark squares, respectively. The insert in Fig. 1a is from Zhang (1997). (b) Schematic map showing major tectonic units and faults of Dabie orogenic belt. NHY, NDC, SDC and SSB represent the North Huaiyang unit, North Dabie complex unit, South Dabie high–ultrahigh-pressure metamorphic complex unit and Susong blueschist unit, respectively (after Suo et al., 2000). (c) Geological map showing early Cretaceous mafic dikes from the NDC and volcanics from the NHY (after Fan et al., 2004; Wang et al., 2002).

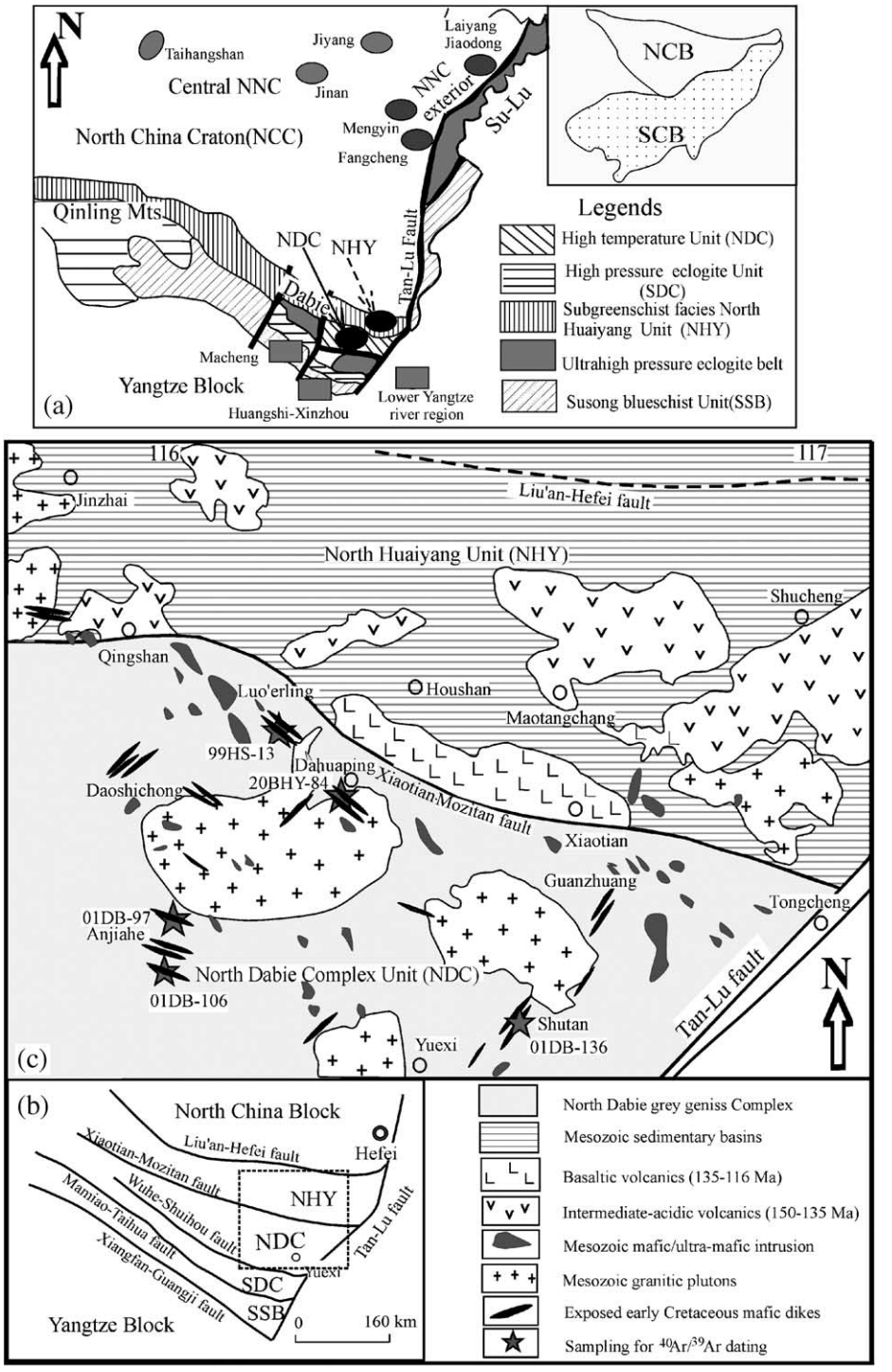
N
Taihangshan
Jiyang
Laiyang
Jiaodong
Central NNC
Jinan
NNC exterior
Su-Lu
Mengyin
North China Craton(NCC)
Fangcheng
NCB
SCB
Qinling Mts
NDC
NHY
Tan-Lu Fault
Dabie
Legends
High temperature Unit (NDC)
High pressure eclogite Unit (SDC)
Subgreenschist facies North Huaiyang Unit (NHY)
Ultrahigh pressure eclogite belt
Susong blueschist Unit(SSB)
Macheng
Yangtze Block
(a)
Huangshi-Xinzhou
Lower Yangtze river region
116
117
Jinzhai
Liu'an-Hefei fault
North Huaiyang Unit (NHY)
Shucheng
Qingshan
Houshan
Luo'erling
Maotangchang
99HS-13
Dahuaping
20BHY-84
Daoshichong
Xiaotian-Mozitan fault
Xiaotian
Guanzhuang
Tongcheng
01DB-97
Anjiahe
North Dabie Complex Unit (NDC)
01DB-106
Shutan
01DB-136
Yuexi
Tan-Lu fault
N
(c)
(b)
North China Block
Liu'an-Hefei fault
Hefei
Xiaotian-Mozitan fault
Wuhe-Shuihou fault
NHY
Mantiao-Taihua fault
NDC
Tan-Lu fault
Yuexi
Xiangfan-Guangji fault
SDC
SSB
Yangtze Block
0
160 km
North Dabie grey geniss Complex
Mesozoic sedimentary basins
Basaltic volcanics (135-116 Ma)
Intermediate-acidic volcanics (150-135 Ma)
Mesozoic mafic/ultra-mafic intrusion
Mesozoic granitic plutons
Exposed early Cretaceous mafic dikes
Sampling for $^{40}Ar/^{39}Ar$ dating

isotopic data for contemporaneous basaltic-andesitic rocks from the NHY. These data, together with elemental and Sr–Nd isotopic compositions for the corresponding samples from the NHY reported by Fan et al. (2004) and Wang et al. (2002), provide new constraints on: (1) the nature of the Mesozoic lithospheric mantle beneath the Dabie Orogen, and (2) the tectonic decoupling of the lithospheric boundary and surface suture between the YB and NCC in the region west of the Tan-Lu fault.

2. Geological background

The Dabie Orogen can be divided into North Huaiyang unit (NHY), North Dabie orthogneiss complexes unit (NDC), South Dabie HP-UHP metamorphic complex unit (SDC) and Susong greenschist/blueschist unit (SSB), which are respectively separated by the Xiaotian-Mozitan fault, Wuhe-Shuihou fault and Mamiao-Taihua fault (Fig. 1b). The general geology of these units has been widely described in literature (e.g. Cong, 1996; Jahn et al., 1999; Hacker et al., 2000; Zhang et al., 2002a,b). Here we only briefly introduce the NHY and NDC where late Mesozoic basic-intermediate rocks occurred.

The NHY is situated to the north of the Xiaotian-Mozitan fault, and is composed dominantly of low-grade metamorphic rocks with minor amphibolite-facies rocks, which were intruded by Cretaceous granitoids and rare mafic/ultramafic intrusions. The unit also contains early Mesozoic detrital rocks (> 1000 m) and voluminous late Mesozoic volcanic-sedimentary sequence (Fig. 1c). The NDC is bounded between the Xiaotian-Mozitan fault in the north and the Wuhe-Shuihou fault in the south. The unit is extensively intruded by Cretaceous granitic plutons and mafic/ultramafic intrusions (Fig. 1c; Jahn et al., 1999; Li and Yan, 2003 and references therein). The presence of eclogites, Mesozoic intermediate-acidic volcanics and mafic dikes in the NDC has recently been reported (Xu et al., 2000; Tsai and Liou, 2000; Wang et al., 2003a).

The Mesozoic volcanic rocks in the Dabie Orogen predominantly developed in Mesozoic volcanic-sedimentary basins in the NHY (Fig. 1c). They consist mainly of mafic to felsic lavas, tuff and volcanic breccias with rarely deformational fabrics. The volcanic sequence uncomfortably overlay pre-J_2 sedimentary and comfortably underlay late Cretaceous strata. Wang et al. (2002) reported that the volcanic sequence is composed of intermediate-acidic Maotangchang Formation (150–135 Ma) and basaltic-andesitic Xiaotian Formation (135–116 Ma), separated by a conglomerate layer (~135 Ma). The basaltic-andesitic rocks from Xiaotian Formation are predominantly basaltic trachyandesites and trachyandesites. Amphibole, clinopyroxene and plagioclase are common phenocrysts. The fine-grained clinopyroxene, plagioclase and minor opaque oxides occur as matrix. Besides the presence of intermediate-acidic volcanic relicts with the ages of 144–136 Ma (equivalent with Maotangchang Formation in the NHY) in the hinterland of NDC (Wang et al., 2003a), there occurred less voluminous mafic dikes free of the deformation and metamorphism. The outcrops of these dikes vary, with thickness from 1 to 15 m and length from 0.5 to 7 km. These mafic dikes dip steeply and cut directly across the grey gneiss, and show WNW- and NE-trending, roughly parallel to the orientations of the Xiaotian-Mozitan and Tan-Lu faults, respectively (Fig. 1c), consisting predominantly of diabase, lamprophyres and trachyandesites, with aphyric to porphyritic textures. Their mineral compositions generally comprised of plagioclase (25–60%), pyroxene (20–50%), biotite (5–15%), amphibole (5%), quartz (1–5%), and minor euhedral sphene, apatite and Fe–Ti oxides. The mafic dikes this paper is concerned with were mainly collected from Lou'erling, Dahuaping, Daoshichong, Anjiahe, Shutan, Yujiawan and Guanzhuang shown on Fig. 1c.

3. Analytical techniques

Whole rock samples were sliced to remove the altered surface and then crushed to millimeter-scale chips. Only fresh chips were selected and cleaned in an ultrasonic bath with de-ionized water. Grains from five samples were carefully handpicked under a binocular microscope, and crushed to 20–40-mesh for $^{40}Ar/^{39}Ar$ analyses. Other rocks chips were powdered to a grain size of <200-mesh by an agate mill for major- and trace-elemental, and Sr–Nd isotopic analyses.

Table 1
$^{40}Ar/^{39}Ar$ isotopic result of incremental heating experiments for mafic rocks from the NDC

Temp °C	$(^{40}Ar/^{39}Ar)_m$	$(^{36}Ar/^{39}Ar)_m$	$(^{37}Ar/^{39}Ar)_m$	$(^{38}Ar/^{39}Ar)_m$	$^{39}Ar_k$ (10^{-12}mol)	$(^{40}Ar/^{39}Ar_k)$ ($\pm 1\sigma$)	$^{39}Ar_k$ %	Apparent age ($t \pm 1\sigma$ Ma)
01DB-106, weight= 0.1368 g, Plateau age: 128.32 ± 0.12 Ma								
420	14.089	0.0193	0.59051	0.0892	5.38	9.213 ± 0.195	2.22	172.34 ± 3.77
550	7.9610	0.0143	0.41789	0.0504	11.31	3.748 ± 0.006	4.68	72.11 ± 0.97
670	8.6145	0.0062	0.37583	0.0298	22.26	6.778 ± 0.006	9.22	128.37 ± 1.68
780	8.0494	0.0042	0.31263	0.0257	32.82	6.798 ± 0.005	13.5	128.75 ± 1.64
900	7.8494	0.0035	0.23614	0.0159	64.71	6.784 ± 0.004	26.8	128.48 ± 1.61
1050	8.2038	0.0048	0.29952	0.0187	47.78	6.770 ± 0.005	19.7	128.23 ± 1.63
1180	8.2905	0.0051	0.47373	0.0304	27.13	6.792 ± 0.005	11.2	128.63 ± 1.66
1300	8.7790	0.0069	0.49857	0.0389	19.94	6.740 ± 0.006	8.26	127.67 ± 1.70
1450	10.837	0.0139	0.56667	0.0644	9.97	6.753 ± 0.011	4.13	127.92 ± 2.01
Inverse isochron age: 129.03 ± 0.22 Ma, $^{40}Ar/^{36}Ar$ ratios=287.2, MSWD=0.93								
01DB-136, weight= 0.1412 g, Plateau age: 129.64 ± 0.20 Ma								
430	16.296	0.0259	0.45313	0.0888	5.64	8.684 ± 0.022	2.58	162.60 ± 4.00
560	9.9632	0.0196	0.43180	0.0629	9.46	4.204 ± 0.009	4.34	80.55 ± 1.21
680	8.8461	0.0065	0.26747	0.0321	21.10	6.900 ± 0.006	9.69	130.37 ± 1.73
800	8.2926	0.0048	0.24123	0.0304	28.53	6.849 ± 0.005	13.1	129.43 ± 1.67
920	7.8571	0.0032	0.14902	0.0188	56.83	6.879 ± 0.005	26.1	129.98 ± 1.63
1050	7.9569	0.0037	0.18196	0.0222	43.14	6.835 ± 0.005	19.8	129.19 ± 1.63
1180	8.4954	0.0055	0.25839	0.0318	25.28	6.869 ± 0.006	11.6	129.80 ± 1.69
1300	9.1139	0.0075	0.31250	0.0386	18.32	6.877 ± 0.007	8.41	129.96 ± 1.76
1450	11.133	0.0147	0.37969	0.0677	9.42	6.791 ± 0.011	4.32	128.39 ± 2.07
Inverse isochron age: 130.49 ± 0.22 Ma, $^{40}Ar/^{36}Ar$ ratios=287.8, MSWD=1.07								
99HS-13, weight= 0.1443 g, Plateau age: 128.23 ± 0.19 Ma								
400	18.095	0.0317	0.68022	0.1042	4.38	8.791 ± 0.027	1.83	164.52 ± 4.78
520	10.000	0.0213	0.46690	0.0682	8.70	3.736 ± 0.010	3.63	71.77 ± 1.10
650	8.6792	0.0062	0.28492	0.0371	18.44	6.824 ± 0.006	7.71	128.99 ± 1.71
780	8.4959	0.0056	0.21601	0.0272	28.53	6.810 ± 0.006	11.9	128.73 ± 1.67
900	7.6459	0.0029	0.33783	0.0180	63.55	6.785 ± 0.004	26.5	128.27 ± 1.60
1000	8.1547	0.0047	0.37169	0.0279	38.96	6.755 ± 0.005	16.3	127.73 ± 1.63
1100	7.9513	0.0041	0.29334	0.0298	33.40	6.721 ± 0.005	13.9	127.10 ± 1.62
1200	8.7280	0.0065	0.36920	0.0411	21.15	6.795 ± 0.006	8.84	128.46 ± 1.72
1300	9.8434	0.0104	0.49615	0.0586	13.33	6.789 ± 0.009	5.57	128.34 ± 1.88
1450	10.756	0.0135	0.43350	0.0745	8.58	6.793 ± 0.011	3.58	128.41 ± 2.05
Inverse isochron age: 127.97 ± 0.22 Ma, $^{40}Ar/^{36}Ar$ ratios=296.3, MSWD=1.30								
01BHY-84, weight= 0.1289 g, Plateau age: 131.83 ± 0.34 Ma								
420	13.828	0.0167	0.44232	0.079	6.24	8.921 ± 0.016	2.63	167.12 ± 3.31
540	8.527	0.0140	0.35015	0.0492	11.57	4.401 ± 0.007	4.89	84.40 ± 1.15
660	8.8535	0.0063	0.26900	0.0354	18.20	6.973 ± 0.006	7.69	131.94 ± 1.75
780	8.5566	0.0057	0.21526	0.0288	28.29	6.866 ± 0.006	11.9	129.99 ± 1.69
900	7.8478	0.0029	0.27444	0.0183	62.51	6.967 ± 0.005	26.4	131.83 ± 1.65
1000	8.4545	0.0048	0.39953	0.0269	38.26	7.032 ± 0.005	16.1	133.03 ± 1.72
1100	8.2042	0.0042	0.33365	0.0292	32.93	6.960 ± 0.005	13.9	131.69 ± 1.69
1200	8.9237	0.0067	0.44463	0.0429	20.68	6.954 ± 0.007	8.74	131.59 ± 1.78
1300	10.198	0.0108	0.56975	0.0601	12.87	7.039 ± 0.009	5.44	133.14 ± 1.99
1450	16.469	0.0284	0.79759	0.1351	4.89	8.152 ± 0.025	2.06	153.31 ± 4.11
Inverse isochron age: 131.35 ± 0.22 Ma, $^{40}Ar/^{36}Ar$ ratios==298.8, MSWD=3.24								

(continued on next page)

Table 1 (*continued*)

Temp °C	$(^{40}Ar/^{39}Ar)_m$	$(^{36}Ar/^{39}Ar)_m$	$(^{37}Ar/^{39}Ar)_m$	$(^{38}Ar/^{39}Ar)_m$	$^{39}Ar_k$ (10^{-12}mol)	$(^{40}Ar/^{39}Ar_k)$ ($\pm 1\sigma$)	$^{39}Ar_k$ %	Apparent age ($t \pm 1\sigma$ Ma)
01DB-97, weight= 0.1333 g, Plateau age: 127.56 ± 0.23 Ma								
400	15.910	0.0242	0.57771	0.1245	6.24	8.831 ± 0.023	2.19	165.23 ± 4.16
520	7.2269	0.0102	0.45378	0.0636	13.59	4.226 ± 0.006	4.77	80.96 ± 1.10
650	8.5353	0.0060	0.37790	0.0439	22.96	6.756 ± 0.006	8.06	127.74 ± 1.70
780	8.1292	0.0047	0.47768	0.0323	34.09	6.739 ± 0.005	11.9	127.43 ± 1.64
900	7.7096	0.0032	0.33049	0.0224	71.90	6.758 ± 0.004	25.2	127.78 ± 1.60
1000	7.9802	0.0039	0.32606	0.0302	47.08	6.819 ± 0.005	16.5	128.89 ± 1.64
1100	7.7710	0.0036	0.42301	0.0349	38.50	6.714 ± 0.005	13.5	126.98 ± 1.62
1200	8.2327	0.0051	0.56068	0.0409	26.90	6.729 ± 0.006	9.44	127.26 ± 1.66
1300	8.8944	0.0075	0.62185	0.0497	18.45	6.701 ± 0.007	6.48	126.74 ± 1.73
1450	16.353	0.0275	0.97689	0.1353	5.05	8.319 ± 0.024	1.77	156.06 ± 4.14
Inverse isochron age: 128.58 ± 0.22 Ma, $^{40}Ar/^{36}Ar$ ratios==280.8, MSWD=2.15								

$\lambda = 5.543 \times 10^{-10}$ /year, $J = 0.01086$.

Five selected $^{40}Ar/^{39}Ar$ samples were individually wrapped in Al-foil packets, encapsulated in sealed Gd-foil, and irradiated in the central thimble position of the nuclear reactor (1000 kW) at the Chinese Academy of Atomic Energy Science for 2627 min with an instantaneous neutron flux of 6.63×10^{12} n/cm^2. Samples were then degassed and purified in steps from 400–420 °C to 1450 °C. Purified argon was analyzed with gas source mass spectrometers RGA-10, and this was conducted in the static mode at the Institute of Geology and Geophysics (IGG), the Chinese Academy of Sciences (CAS). The concentrations of ^{36}Ar, ^{37}Ar, ^{38}Ar, ^{39}Ar and ^{40}Ar were corrected for system blank, radioactive decay of nucleogenic isotopes, and minor interference reactions involving Ca, K and Cl. The detailed analytical and correction techniques have been described by Sang et al. (1996). The internal standard Biotite ZBH-25 monitor yielded the age of 132.7 ± 1.2 Ma. The analytical results are presented in Table 1.

Major elements were determined by a wavelength dispersive X-ray fluorescence spectrometry at the Hubei Institute of Geology and Mineral Resource, the Chinese Ministry Land and Resource. FeO content in samples was solely analyzed by a wet-chemical method. The relative standard derivations (RSD) are within 5%, and totals are 100 ± 1%. The analytical results of GSR-2 and GSR-3 international standard are reported by Fan et al. (2004). Trace element analyses were performed at the Institute of Geochemistry, CAS using an inductively coupled plasma mass spectrometry (ICP-MS). About 100-mg samples are digested with 1 ml of HF and 0.5 ml HNO_3 in screw top PTFE-lined stainless steel bombs at 190 °C for 12 h. Insoluble residues are dissolved using 8 ml of 40% HNO_3 (v/v) heated to 110 °C for 3 h. Rh and In are used as internal standard for correcting instrumental signal drift, which was usually <10% over a period of 6 h. Detailed sample preparation and analytical procedure follows Qi et al. (2000). The analytical precision is better than 5% for elements >10 ppm, less than 8% for those <10 ppm, and about 10% for transition metals from repetitive analyses of BHVO-1 (Xu, 2002), AMH-1 and OU-3 international standards whose measured and reference values are listed in Table 2. The analytical results of the samples are listed in Table 2.

Sample powders for Sr and Nd isotopic analyses were spiked with mixed isotope tracers, dissolved in Teflon beakers with HF + HNO_3 acids, and separated by a conventional cation exchange technique and run on single W and Ta–Re double filaments, respectively. The total procedure blanks are in the range of 200–500 pg for Sr and less than 50 pg for Nd and are negligible. Isotopic measurement was performed on the VG-354 mass-spectrometer at the IGG, CAS. The mass fractionation corrections for Sr and Nd isotopic ratios were based on $^{86}Sr/^{88}Sr = 0.1194$ and $^{146}Nd/^{144}Nd = 0.7219$, respectively. $^{87}Sr/^{86}Sr$ ratio of the NBS 987 standard and $^{143}Nd/^{144}Nd$ ratio of the La Jolla standard measured were 0.710265 ± 12 (2σ) and 0.511862 ± 10 (2σ) respectively. $^{87}Rb/^{86}Sr$ and $^{147}Sm/^{144}Nd$ ratios were calculated using the Rb, Sr, Sm and Nd abun-

dances measured by ICP-MS. For Pb isotopic determination, about 100 mg powder was weighted into the Teflon beaker, spiked and dissolved in concentrated HF at 180 °C for 7 h. Pb was separated and purified by conventional cation-exchange technique (AG1 × 8, 200–400 resin) with diluted HBr as an eluant. Total procedure blanks were less than 50 pg Pb. Detailed descriptions of the analytical techniques are given by Zhang et al. (2002a,b). Isotopic ratios were measured with the VG-354 mass-spectrometer at the IGG, CAS. Repeated analyses of NBS 981 yielded the average values of $^{206}Pb/^{204}Pb = 16.942 \pm 4$ (2σ), $^{207}Pb/^{204}Pb = 15.498 \pm 4$ (2σ) and $^{208}Pb/^{204}Pb = 36.728 \pm 9$ (2σ). External precisions are estimated to be less than 0.005, 0.005 and 0.0015. The Sr–Nd and Pb results are presented in Tables 3 and 4, respectively.

4. Results

4.1. $^{40}Ar/^{39}Ar$ geochronology

Five samples (01DB-106, 01DB-136, 01DB-97, 20BHY-84, 99HS-13) were collected from the central locations of five aplitic diabases (~10 m wide) in the NDC. The sampling locations are shown in Fig. 1c and the age spectra are given in Fig. 2a–c. These samples yielded the $^{40}Ar/^{39}Ar$ plateau ages of 128.3 ± 0.1 Ma (01DB-106), 129.6 ± 0.2 Ma (01DB-136), 127.6 ± 0.2 Ma (01DB-97), 128.2 ± 0.2 Ma (99HS-13) and 131.8 ± 0.3 Ma (20BHY-84), respectively. These plateau ages are defined by > 89% of total ^{39}Ar released with invariability for at 1σ level of uncertainty. In the correlation of $^{36}Ar/^{40}Ar$ versus $^{39}Ar/^{40}Ar$ diagrams (Fig. 2a′–e′), the data of each sample define a linear array with acceptable values of the mean square of the weight deviates (MSWD). Their intercept ages and $^{40}Ar/^{36}Ar$ initial ratios (280.8–298.8) are consistent with their respective plateau ages and the present atmospheric $^{40}Ar/^{36}Ar$ ratio (295.5), thus the excess argon is insignificant and the plateau ages (127.6–131.8 Ma) are reliable. The plateau ages can be interpreted to be the intrusive ages of these mafic dikes, which are similar to those of the mafic/ultramafic intrusions in the Dabie Orogen (~125 Ma, Jahn et al., 1999) and the basaltic-andesitic rocks from the Xiaotian Formation in the NHY (135–116 Ma, Wang et al., 2002).

4.2. Elemental geochemistry

The mafic dikes from the NDC have SiO_2 of 51.80–55.92%, MgO of 3.30–7.30%, and TiO_2 = 1.38–1.64% with K_2O/Na_2O of 0.82–1.66, consistent with basaltic trachyandesites (Table 2 and Fig. 3a). They are relatively high in *mg*-numbers (= Mg/(Mg + ΣFe) in atomic ratio) (0.41–0.61) and transition metals (V = 102–186 ppm, Cr = 51–299 ppm, Ni = 25–100 ppm). The rocks from the Xiaotian Formation in the NHY exhibit slightly higher SiO_2 (53.41–58.81%), and lower MgO (2.51–6.84%), TiO_2 (1.28–1.56%) and K_2O (3.06–4.70%) contents than those from the NDC, thus are basaltic trachyandesites and trachyandesites (Fig. 3a). These rocks from the NHY have similar *mg* number (0.44–0.65) and transition metals (Cr = 90–208 ppm, Ni = 39–83 ppm) as those from the NDC (Fan et al., 2004; Wang et al., 2002). In the Harker diagrams (Fig. 3a–g), these samples from both tectonic units form a continuous array. In general, SiO_2 inversely correlates with MgO, Al_2O_3, CaO, FeOt, TiO_2 and P_2O_5. Transition metals (Cr, Co, Ni) drastically decrease with decreasing MgO (Fig. 3i–j).

As to incompatible element abundances, the rocks from the NDC are enriched in rare-earth elements (REE) and show strong LREE/HREE fractionation ((La/Yb)cn = 10.1–27.1) with Eu/Eu* = 0.74–1.02 (Table 2). The rocks from the NHY have an even stronger LREE enrichment ((La/Yb)cn = 27.7–35.9) with slightly negative Eu anomalies (Eu*/Eu = 0.68–0.90) than those from the NDC. These samples are generally enriched in large-ion lithophile elements (LILEs) and depleted in high-field strength elements (HFSEs). On the primitive mantle normalized diagrams (Fig. 4a–b), these samples from both tectonic units are characterized by subparallel patterns with pronounced depletion of Nb–Ta–Ti. (Nb/La)n ratio is in the range of 0.24–0.47 for the rocks from the NDC and (Nb/La)n = 0.21–0.30 for those from the NHY. Th and U are slightly depleted relative to La (0.57–0.93). In Fig. 4a, weakly Sr anomalies for some samples from the NDC are also apparent. These features are generally similar to those of Mesozoic basaltic rocks from the NCC exterior (i.e., the Laiyang and Fangcheng areas; Fan et al., 2001; Zhang et al., 2002a,b), but distinctive from the Mesozoic mafic rocks of the Yangtze interior (e.g., Wang et al., 2003b).

Table 2
Major and trace elemental data of early Cretaceous mafic dikes from the NDC

Sample	AMH-1		OU-3		20BHY-85	01DB-97	01DB-99	01DB-106	01DB-108	01DB-134	01DB-136
Group 1	this work (n=6)	Ref.	this work (n=6)	Ref.	Anjiahe			South Anjiahe		Shutan, Nishui	
wt.%											
SiO_2					50.99	50.87	50.04	51.39	53.02	52.71	51.51
Al_2O_3					15.70	15.99	15.68	15.81	15.28	14.78	14.88
Fe_2O_3					3.05	3.28	3.19	2.61	3.27	1.90	1.96
FeO					4.58	4.87	4.77	5.42	4.43	5.57	5.57
MgO					5.67	4.56	4.52	4.72	3.84	6.19	6.32
CaO					6.95	5.67	5.58	6.20	4.49	6.86	6.44
Na_2O					2.99	3.13	3.15	3.60	4.51	3.02	3.47
K_2O					3.65	4.99	4.42	3.95	3.80	3.73	2.97
MnO					0.11	0.15	0.13	0.13	0.11	0.14	0.14
TiO_2					1.36	1.53	1.48	1.47	1.40	1.32	1.34
P_2O_5					0.94	1.17	1.15	1.11	0.98	0.55	0.56
LOI					3.30	3.12	5.35	3.02	3.87	3.12	4.59
Total					99.29	99.33	99.46	99.43	99.30	99.89	99.75
mg					0.58	0.51	0.52	0.52	0.49	0.60	0.61
ppm											
Sc	13.9 ± 0.2	13.5	4.76 ± 0.2		19.0	14.6	15.1	14.6	11.9	16.7	16.8
V	114 ± 3	106	1.1 ± 0.1		162	147	155	146	115	105	115
Cr	41 ± 3	40.9	16.7 ± 0.5	18.6	140	59.9	51.0	57.3	42.0	273	268
Co	19.5 ± 0.3	18.7	0.37 ± 0.02		28.4	34.0	34.4	36.1	28.9	39.8	42.0
Ni	35.0 ± 0.6	32.4	1.51 ± 0.02		69.8	59.1	55.6	60.7	44.3	35.2	50.9
Rb	18.3 ± 0.2	18.3	168 ± 3	172	88	129	106	89	85	73	61
Sr	562 ± 4	545	11.0 ± 0.2	11.2	1112	1009	820	553	672	575	520
Y	15.2 ± 0.2	16.4	110 ± 2	113	25.8	28.8	29.8	30.8	27.8	22.0	22.2
Zr	139 ± 5	146	951 ± 11	943	293	324	343	319	381	227	218
Nb	8.4 ± 0.2	8.32	82.2 ± 1.0	80.3	23.59	26.98	27.46	25.80	29.96	13.46	13.67
Ba	315 ± 10	322	27.1 ± 0.3	28.8	3433	4598	3624	3809	2443	1208	942
La	16.22 ± 0.15	15.87	92.6 ± 1.0	94.6	82.2	91.46	93.1	88.34	93.8	34.0	35.4
Ce	34.50 ± 0.30	33.03	198.3 ± 2.0	196.3	160.1	179.3	187.2	173.4	184.5	68.0	70.4
Pr	4.20 ± 0.10	4.21	22.5 ± 0.20	22.7	17.97	20.28	20.93	19.53	19.99	7.45	7.77
Nd	17.9 ± 0.2	17.69	89.0 ± 1.0	87.0	67.27	82.43	87.20	80.25	79.50	30.48	32.27
Sm	3.80 ± 0.10	3.68	19.23 ± 0.15	18.72	10.83	13.71	14.14	13.98	13.38	5.96	6.14
Eu	1.08 ± 0.05	1.16	1.12 ± 0.02	1.15	2.48	3.13	3.00	3.12	2.82	1.79	1.84
Gd	3.48 ± 0.06	3.34	17.81 ± 0.17	18.07	7.69	8.88	9.20	9.19	8.58	5.26	5.15
Tb	0.52 ± 0.01	0.51	3.28 ± 0.04	3.08	0.97	1.10	1.18	1.18	1.14	0.78	0.76
Dy	3.0 ± 0.03	2.84	19.5 ± 0.4	18.87	5.02	6.01	6.04	6.00	6.01	4.61	4.48
Ho	0.58 ± 0.10	0.57	4.01 ± 0.07	4.01	0.85	1.19	1.27	1.30	1.23	0.88	0.94
Er	1.54 ± 0.03	1.52	11.90 ± 0.15	11.45	2.45	2.98	2.98	3.07	2.92	2.25	2.22
Tm	0.22 ± 0.02	0.21	1.72 ± 0.02	1.73	0.35	0.43	0.43	0.39	0.37	0.32	0.32
Yb	1.35 ± 0.05	1.37	11.88 ± 0.10	11.38	2.17	2.89	2.94	2.74	2.74	2.26	2.15
Lu	0.22 ± 0.01	0.21	1.58 ± 0.02	1.63	0.31	0.40	0.40	0.38	0.35	0.26	0.31
Hf	3.80 ± 0.10	3.70	23.02 ± 0.30	22.60	7.72	6.91	7.26	7.31	8.56	4.74	4.67
Ta	0.60 ± 0.10	0.64	5.69 ± 0.10	5.75	1.07	1.34	1.46	1.35	1.61	1.18	1.12
Pb	9.85 ± 0.10	10.02	35.19 ± 0.70	36.25	11.72	16.60	15.53	13.50	19.10	15.55	13.50
Th	2.61 ± 0.02	2.64	22.40 ± 0.50	22.84	9.01	8.21	8.73	8.07	9.23	3.52	3.23
U	0.91 ± 0.03	0.89	5.52 ± 0.08	5.54	1.39	1.51	1.61	1.41	1.50	0.93	1.02
Nb/La					0.29	0.30	0.29	0.29	0.32	0.48	0.47
Ba/Nb					145.5	170.4	132.0	147.07	81.50	73.4	56.5
(La/Yb)cn					25.58	21.39	21.41	21.82	23.17	10.18	11.13
(Gd/Yb)cn					2.87	2.49	2.54	2.72	2.54	1.89	1.94
Eu/Eu*					0.79	0.81	0.76	0.79	0.75	0.96	0.98

LOI: Loss ion ignition, $mg = Mg^{2+}/(Mg^{2+} + Fe^{2+})$; Reference values of AMH-1 and OU-3 international standard are from Thompson et al. (2000) and Potts et al. (2000).

01DB-138	01DB-152	01DB-162	99HS-11	99HS-12	99HS-13	99HS-14	20BHY-81	20BHY-86	20BHY-82	20BHY-83	20BHY-84
	Yujiawan	Guanzhuang	Lou'erling				Dahuaping			Daoshichong	
52.22	53.39	51.54	51.75	50.34	49.14	50.21	50.72	49.34	50.52	52.15	49.32
14.70	15.53	14.72	15.49	15.59	15.26	15.74	15.36	15.22	15.67	15.90	15.78
1.67	3.21	3.04	2.47	2.68	3.14	2.36	3.19	3.08	3.43	3.38	3.00
5.82	5.35	5.58	5.61	5.90	5.16	6.39	4.56	4.88	4.62	4.45	4.95
6.34	3.16	6.67	5.73	5.81	6.85	6.71	5.18	5.55	5.37	4.39	5.96
6.63	5.76	7.61	5.96	5.76	5.75	5.32	7.43	6.47	7.62	6.89	7.37
3.10	3.92	2.63	3.29	2.91	3.05	2.76	2.49	2.80	2.85	2.97	2.53
3.09	3.24	3.46	3.39	3.84	3.31	3.81	4.13	4.12	3.55	3.77	3.73
0.16	0.13	0.15	0.11	0.11	0.11	0.12	0.11	0.13	0.14	0.11	0.12
1.36	1.37	1.38	1.37	1.43	1.42	1.42	1.43	1.42	1.47	1.52	1.44
0.55	0.65	0.93	0.57	0.89	0.88	0.88	0.98	0.99	1.00	1.15	1.00
4.12	3.83	2.74	3.94	4.04	5.60	3.61	3.66	5.27	3.01	2.69	4.05
99.76	99.64	99.45	99.68	99.30	99.67	99.33	99.25	99.28	99.34	99.45	99.39
0.61	0.41	0.59	0.57	0.55	0.61	0.58	0.56	0.57	0.56	0.51	0.58
17.6	10.8	23.6	17.8	16.8	18.3	20.3	18.4	18.7	19.4	16.5	20.4
121	103	186	173	176	185	161	159	162	169	152	172
299	11.2	196	128	150	142	239	144	139	147	64.3	142
43.0	33.7	45.0	32.3	36.7	32.2	39.5	27.6	28.5	30.4	23.5	29.3
55.7	55.2	76.5	59.7	72.9	64.4	100	69.5	67.2	73.1	42.7	71.3
64	84	80	100	105	102	107	114	118	94	109	116
534	678	792	370	377	709	358	709	734	966	683	773
25.0	29.0	27.7	22.7	26.0	22.6	26.2	26.3	24.9	27.1	29.2	25.9
223	279	339	288	302	300	302	287	282	296	369	284
13.53	13.56	14.89	19.20	19.87	19.60	19.58	22.63	21.73	23.11	25.06	22.48
675	1717	2424	1073	1016	1550	1401	3287	4064	3336	2908	3195
37.2	49.8	53.0	51.4	53.3	53.6	55.0	82.2	78.8	85.1	99.1	83.9
72.6	98.6	107.0	103.5	108.0	109.1	110.6	160.3	156.1	165.7	197.3	163.1
8.21	11.22	12.30	11.61	11.83	12.33	12.24	17.62	17.47	18.42	20.97	17.74
33.67	47.88	53.02	44.33	45.20	45.01	45.67	66.56	66.36	70.00	82.53	70.10
6.42	9.47	10.74	9.07	9.36	9.21	9.56	10.78	10.21	11.57	13.05	10.96
1.99	2.57	2.58	2.21	2.32	2.35	2.15	2.50	2.42	2.48	3.06	2.51
5.28	7.21	7.82	7.07	7.37	6.94	7.39	7.49	7.56	8.17	9.15	7.79
0.85	1.06	1.11	0.89	1.03	0.89	1.02	0.95	0.96	1.04	1.17	1.02
4.86	5.71	5.74	5.01	5.61	5.29	5.59	4.81	4.92	5.07	5.78	5.22
1.02	1.14	1.17	0.87	0.98	0.88	1.09	0.90	0.89	0.96	1.05	0.91
2.56	3.11	2.83	2.25	2.56	2.48	2.86	2.43	2.31	2.51	2.75	2.65
0.33	0.43	0.39	0.33	0.38	0.30	0.37	0.35	0.33	0.35	0.37	0.34
2.50	2.77	2.79	2.01	2.47	1.96	2.50	2.05	2.18	2.15	2.41	2.20
0.28	0.36	0.35	0.28	0.33	0.28	0.37	0.29	0.31	0.29	0.33	0.28
4.90	6.15	8.41	6.76	7.39	7.42	7.32	7.05	6.95	7.40	9.19	7.11
1.24	1.10	0.75	0.99	1.03	1.03	0.96	1.01	1.01	1.07	1.14	1.05
12.43	14.16	12.98	14.16	12.85	12.85	12.85	11.87	9.99	11.53	14.13	10.46
3.57	3.51	5.18	5.84	5.77	5.68	5.67	8.85	8.14	8.94	9.19	9.17
0.89	0.94	1.05	1.23	1.31	1.12	1.34	1.31	1.24	1.31	1.30	1.44
0.44	0.37	0.28	0.37	0.37	0.37	0.36	0.28	0.28	0.27	0.25	0.27
40.8	92.47	229.98	55.88	51.12	79.08	71.57	145.25	186.98	144.36	116.05	142.12
10.05	12.13	12.84	17.25	14.60	18.46	14.88	27.13	24.43	26.69	27.77	25.74
1.71	2.11	2.27	2.85	2.42	2.87	2.40	2.97	2.81	3.07	3.08	2.87
1.02	0.91	0.82	0.81	0.83	0.86	0.75	0.81	0.81	0.74	0.81	0.79

Table 3
Sr and Nd isotopic data of early Cretaceous mafic dikes from the NDC and contemporaneous basaltic-andesitic rocks from the NHY

Sample	Sm	Nd	Rb	Sr	$^{147}Sm/^{144}Nd$	$^{143}Nd/^{144}Nd \pm 2\sigma$	$^{87}Rb/^{86}Sr$	$^{87}Sr/^{86}Sr \pm 2\sigma$	$(^{87}Sr/^{86}Sr)_i$	$\varepsilon_{Nd}(t)$
Mafic dikes from the NDC (~129 Ma)										
99HS-11	9.07	44.33	99.52	369.7	0.124	0.511838 ± 12	0.780	0.709900 ± 17	0.708458	−14.40
99HS-13	9.21	45.01	102.02	709.1	0.124	0.511842 ± 13	0.417	0.708071 ± 16	0.707300	−14.32
99HS-14	9.56	45.67	106.78	358.4	0.127	0.511828 ± 10	0.864	0.709631 ± 18	0.708035	−14.64
20BHY-81	10.78	66.56	113.95	708.9	0.098	0.511782 ± 11	0.466	0.709040 ± 20	0.708179	−15.06
20BHY-84	10.96	70.10	116.39	773.4	0.095	0.511840 ± 15	0.436	0.708802 ± 20	0.707996	−13.88
20BHY-86	10.21	66.36	117.84	734.0	0.093	0.511770 ± 12	0.465	0.708999 ± 20	0.708139	−15.22
01DB-97	13.71	72.43	129.25	1009	0.114	0.511801 ± 14	0.371	0.708982 ± 17	0.708296	−14.97
01DB-106	13.98	70.25	88.88	553.4	0.120	0.511776 ± 13	0.466	0.708845 ± 18	0.707985	−15.55
01DB-134	5.96	30.48	72.60	575.2	0.118	0.511884 ± 11	0.366	0.708003 ± 15	0.707327	−13.41
01DB-136	6.14	32.27	60.78	519.9	0.115	0.511939 ± 13	0.339	0.708219 ± 22	0.707593	−12.70
01DB-152	9.47	47.88	84.36	677.7	0.120	0.511596 ± 9	0.361	0.708770 ± 20	0.708103	−19.05
01DB-162	10.74	53.02	80.29	792.2	0.123	0.511688 ± 14	0.294	0.708409 ± 18	0.707866	−17.31
Basaltic-andesitic rocks from the NHY (135-116 Ma)										
99XT-1*	12.63	69.55	117.50	1228	0.110	0.511603 ± 11	0.277	0.708975 ± 15	0.708443	−18.70
99XT-2*	12.60	71.36	89.40	974.4	0.107	0.511601 ± 7	0.266	0.708937 ± 15	0.708427	−18.69
99XT-3*	12.69	71.93	87.24	1052	0.107	0.511588 ± 8	0.240	0.708759 ± 16	0.708298	−18.94
99XT-4*	12.92	72.63	75.29	980.2	0.108	0.511678 ± 9	0.223	0.708848 ± 20	0.708421	−17.20
99XT-11*	12.36	67.72	65.44	782.6	0.110	0.511589 ± 7	0.242	0.708820 ± 13	0.708355	−18.98
99XT-15*	12.28	70.77	102.71	1002	0.105	0.511583 ± 6	0.297	0.708519 ± 17	0.708029	−19.23
20BHY-13	12.34	73.22	78.3	1009	0.102	0.511722 ± 7	0.223	0.707791 ± 20	0.707362	−16.22
20BHY-14	12.49	70.34	79.2	955.1	0.107	0.511692 ± 9	0.241	0.708221 ± 20	0.707764	−16.91

The data marked by * are from Fan et al. (2004) and Wang et al. (2002). Chondrite uniform reservoir values, $^{147}Sm/^{144}Nd = 0.1967$, $^{143}Nd/^{144}Nd = 0.512638$, are used for the calculation. $\varepsilon_{Nd}(t)$ is calculated by assuming 130 Ma for mafic dikes from the NDC and basaltic-andesitic rocks from the NHY. Sm, Nd, Rb and Sr contents: ppm.

4.3. Sr–Nd–Pb isotopes

The rocks from the NDC have high initial $^{87}Sr/^{86}Sr$ ratios (0.70733–0.70990) and low $\varepsilon_{Nd}(t)$ values (−12.7 to −19.1), which are comparable to those from the NHY ($^{87}Sr/^{86}Sr(t) = 0.70736–0.70844$ and $\varepsilon_{Nd}(t) = -16.2$ to −19.2; Wang et al., 2002; Fan et al., 2004). The Sr–Nd isotopic range (Fig. 5) is also similar to those for Cretaceous mafic/ultramafic intrusions in the Dabie Orogen ($^{87}Sr/^{86}Sr(t) = 0.7067–0.7080$, $\varepsilon_{Nd}(t) = -11.0$ to −20.5; Jahn et al., 1999; Li and Yan, 2003), and the Mesozoic basaltic rocks from the NCC exterior (Laiyang basalts and high-*mg* diorites in the Mengyin area; Fan et al., 2001; Wu et al., 2003), but is in contrast to those for Mesozoic mafic rocks from the Yangtze interior (Wang et al., 2003b; Li et al., 2003) and Central NCC (Chen and Zhai, 2003; Guo et al., 2001; Zhang et al., 2004). In comparison with the Fangcheng basalts (Zhang et al., 2002a,b) and K-rich rocks in the Mengyin area (Qiu et al., 2002) in the NCC exterior, these samples from the NDC and NHY have similar $\varepsilon_{Nd}(t)$ values but lower initial $^{87}Sr/^{86}Sr$ ratios.

The rocks from both tectonic units have very similar Pb isotopic compositions (Table 4 and Fig. 6a–b). The samples from the NDC have $(^{206}Pb/^{204}Pb)_i = 15.97–16.98$, $(^{207}Pb/^{204}Pb)_i = 15.27–15.41$ and $(^{208}Pb/^{204}Pb)_i = 36.70–37.62$, and those from the NHY display $(^{206}Pb/^{204}Pb)_i = 16.43–16.95$, $(^{207}Pb/^{204}Pb)_i = 15.32–15.37$, and $(^{208}Pb/^{204}Pb)_i = 37.19–37.71$. All the samples are characterized by very low U/Pb ratios and nonradiogenic Pb isotopes with prominent positive Δ8/4 (146.7–179.5) and Δ7/4 (3.2–8.2). It is noted that such lead isotopic signatures are similar to those of the Fangcheng basalts and Jiaodong mafic rocks from the NCC exterior, but show slightly higher $^{207}Pb/^{204}Pb$ and $^{208}Pb/^{204}Pb$ ratios than those of the Jinan gabbro. In the $(^{206}Pb/^{204}Pb)_i$ versus $(^{207}Pb/204Pb)_i$ and $(^{208}Pb/^{204}Pb)_i$ diagrams (Fig. 6a,b), these samples are plotted to the left side of the north hemisphere reference line (NHRL; Hart, 1984), suggesting more radiogenic ^{207}Pb and ^{208}Pb values than ^{206}Pb.

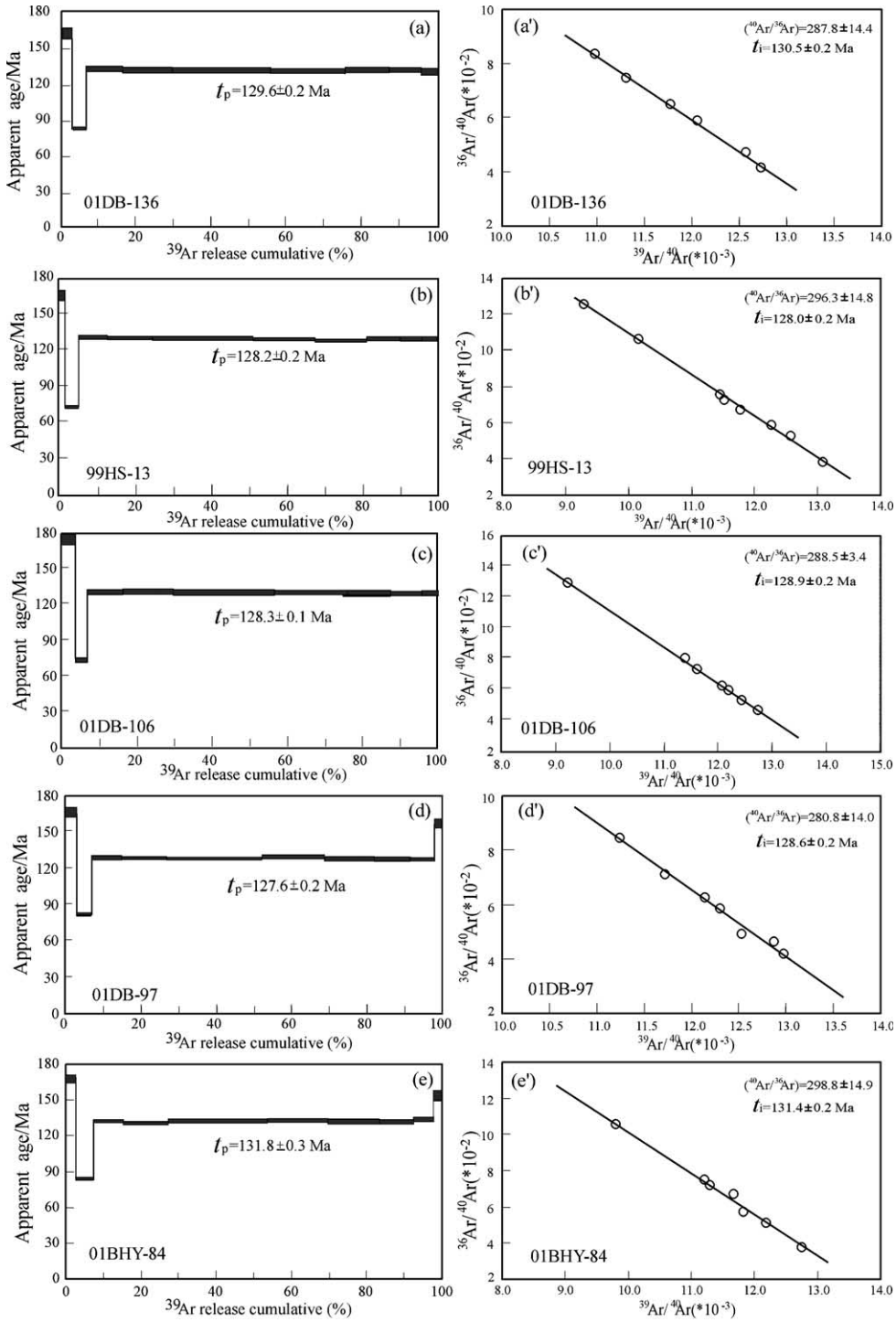

Fig. 2. The ^{40}Ar/^{39}Ar age spectra (a–e) and ^{36}Ar/^{40}Ar versus ^{39}Ar/^{40}Ar diagrams (a′–e′) of five diabases from the NDC. The length of bars reflects 1σ uncertainty. See Fig. 1c for locations of the samples.

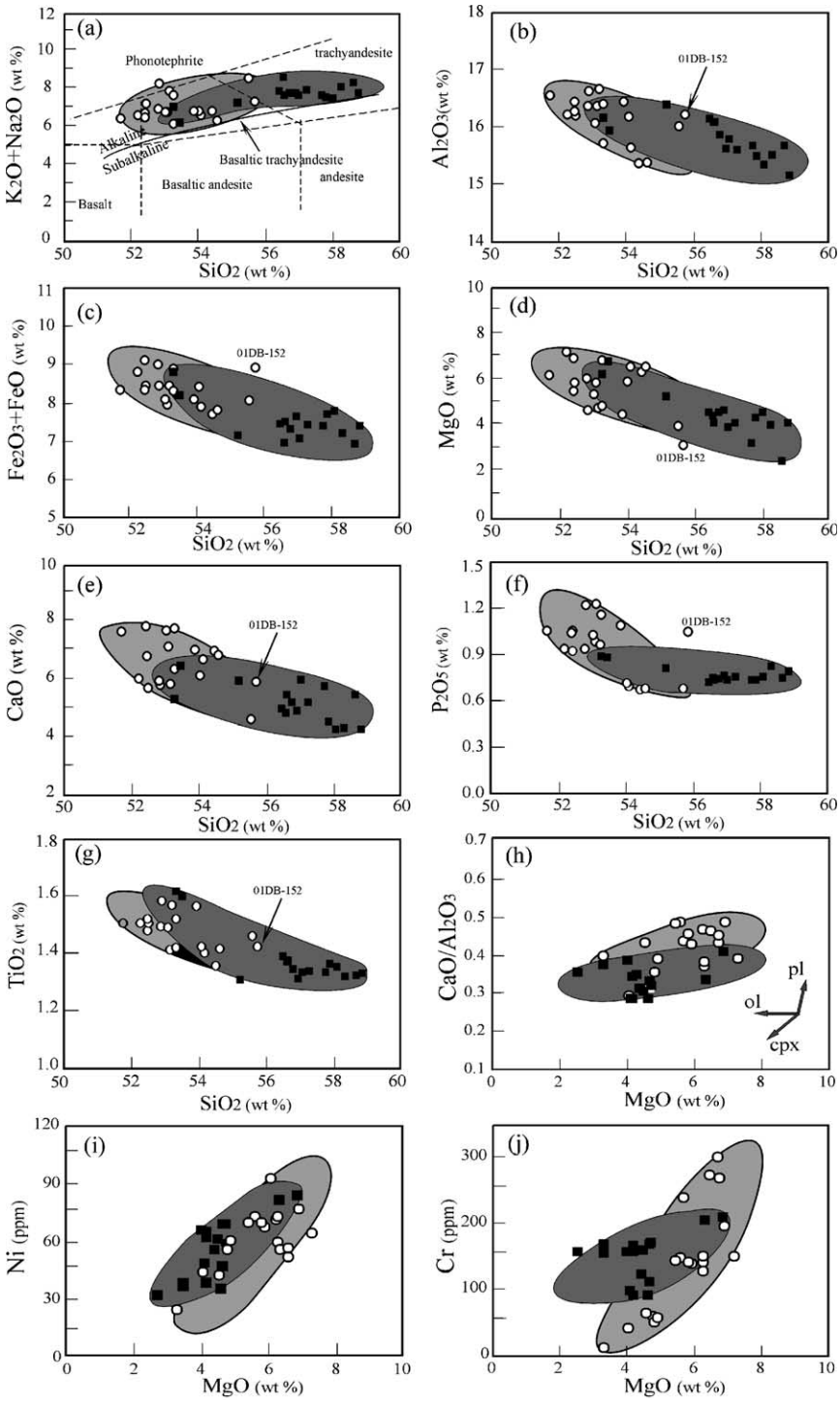

Fig. 3. Plots of SiO_2 versus major oxides (a–g), CaO/Al_2O_3 (h), Ni (i) and Cr (j). The classification scheme in (a) is after Middlemost (1994). The oxides are normalized to 100 wt.% by volatile-free. The data for basaltic-andesitic rocks from the NHY with filled square symbols are from Fan et al. (2004) and Wang et al. (2002). Circle represents mafic rocks from the NDC.

5. Discussion

5.1. Evaluation of magma differentiation

It is essential to evaluate whether or not these samples have undergone low-temperature alteration and crustal assimilation before exploring their mantle sources. These samples might have been subjected to various degrees of alteration viewed from their contents of high loss on ignition (LOI, 2.69–5.60% for the samples from the NDC and 2.10–3.49% for the NHY). However, the consistency of the data set in the primitive mantle-normalized patterns shown in Fig. 4a–b, in combination with the lack of correlation among Na_2O, K_2O, Sr–Nd–Pb isotopic ratios and LOI indicate that the alteration effects on the elements and isotopic ratios are insignificant.

Insignificant crustal assimilation en route for the rocks from the NHY has been discussed by Fan et al. (2004). Our focus here is to evaluate crustal

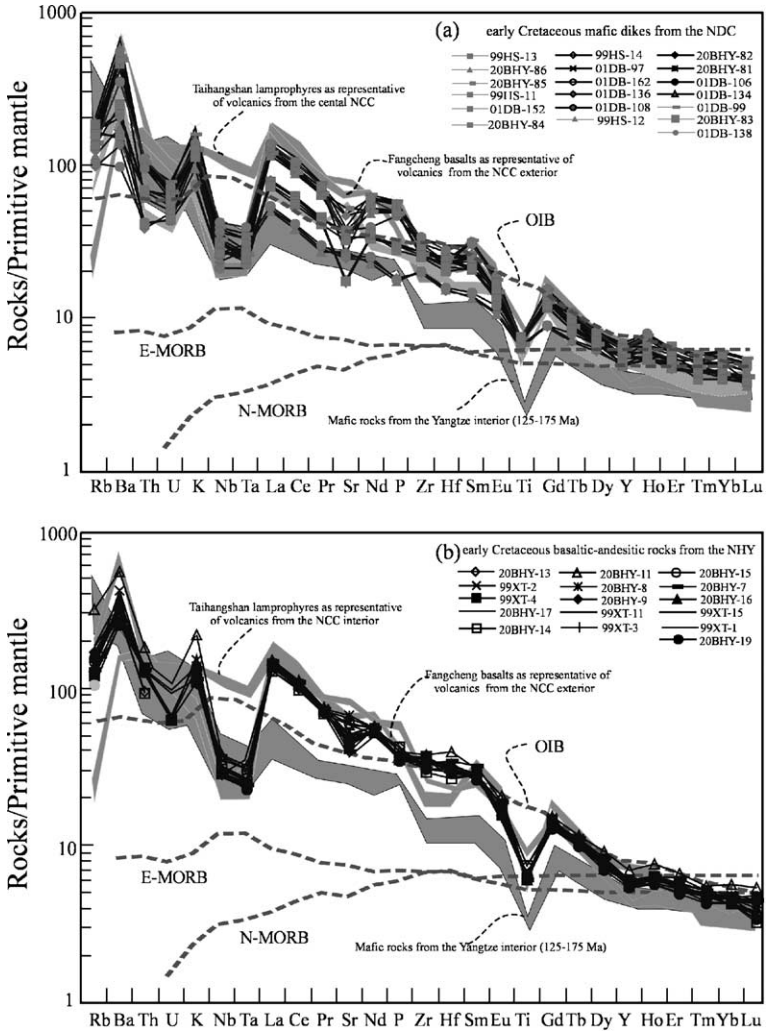

Fig. 4. Primitive mantle-normalized incompatible element patterns for early Cretaceous mafic dikes from the NDC and basaltic-andesitic rocks from the NHY. Normalizing values, OIB, N-MORB and E-MORB are from Sun and McDonough (1989). Data of the Fangcheng basalts as representative of volcanics from the NCC exterior, early Cretaceous Taihangshan lamprophyres as representative of mafic rocks from the Central NCC, and Mesozoic mafic rocks from the Yangtze interior are from Zhang et al. (2002a,b), Chen and Zhai (2003) and Wang et al. (2003b), respectively. Data of basaltic-andesitic rocks from the NHY are from Fan et al. (2004) and Wang et al. (2002).

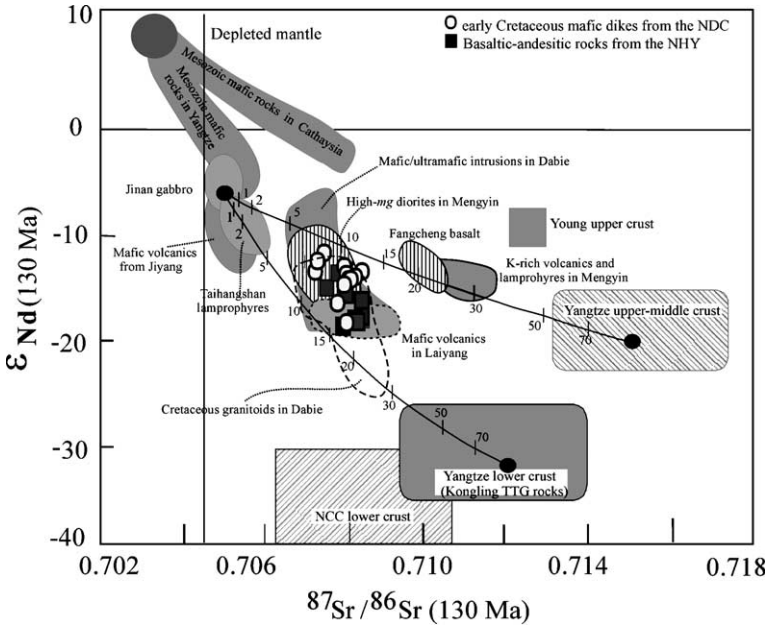

Fig. 5. Initial $^{87}Sr/^{86}Sr(t)$ versus $\varepsilon_{Nd}(t)$ (t=130 Ma) diagram for early Cretaceous mafic dikes from the NDC and contemporaneous basaltic-andesitic rocks from the NHY. Data of the mafic volcanics for the Central NCC (i.e., basaltic rocks for Jiyang basin, mafic dikes for Taihangshan and Jinan gabbros) are from Fan et al. (2001), Guo et al. (2001), Chen and Zhai (2003) and Zhang et al. (2004). Data of Cretaceous mafic/ultramafic intrusions in the Dabie and mafic rocks from the NCC exterior (i.e., Laiyang volcanics, Fangcheng basalts, Mengyin K-rich volcanics, lamprophyres and high-*mg* diorites) are from Jahn et al. (1999), Li and Yan (2003), Zhang et al. (2002a,b), Qiu et al. (2002) and Wu et al. (2003). Kongling TTG rocks are from Gao et al. (1999). Mesozoic mafic rocks in the Yangtze and Cathaysian blocks are from Wang et al. (2003b) and Li et al. (2003). Depleted mantle and Young crust are from Sun and McDonough (1989) while the NCC lower crust and Yangtze upper/middle from Jahn et al. (1999). The numbers indicate the percentages of participation of the crustal materials. The calculated parameters of Sr (ppm), $^{87}Sr/^{86}Sr(t)$, Nd (ppm) and $\varepsilon_{Nd}(t)$ are 60, 0.7050, 4 and −7 for Jinan gabbro source (representative of the NCC lithospheric mantle); 200, 0.7120, 29 and −33 for Kongling TTG rocks (representative of the Yangtze lower crust) and, 220, 0.7150, 20 and −20 for the Yangtze upper/middle crust, respectively (Zhang et al., 1994, 2002a,b; 2004; Gao et al., 1999; Ma et al., 1998, 2000; Chen and Jahn, 1998; Guo et al., 2001; Chen and Zhai, 2003). Same parameters are also used for calculation in Fig. 6c–d and Fig. 7a–b. Locations for mafic rocks from different areas are shown in Fig. 1a.

assimilation for the rocks from the NDC during magma ascend. Assuming that the pre-existing mantle-derived magma can be represented by the Jinan gabbro with SiO_2=52 wt.%, Nd=45 ppm, Sr=800 ppm, $^{87}Sr/^{86}Sr(t)$=0.7050, and $\varepsilon_{Nd}(t)$=−7.0 (Guo et al., 2001; Zhang et al., 2004). The equivalent of crustal assimilation materials can be regarded as a mixture of 40% Yangtze upper/middle crust (SiO_2=76 wt.%) and 60% Yangtze lower crust (SiO_2=59 wt.%). Our modeling calculation suggests that an unrealistic proportion of crustal assimilation (>50%) was required to produce the geochemical variations for the rocks from the NDC (Fig. 7a–b). The (Nb/La)n ratios for the samples are slightly variable (0.21–0.39) irrespective of SiO_2 content (Fig. 8a), near or even lower than that of average continental crust. Th and U contents are weakly depleted relative to LREE, with $(Th/La)_{PM}$=0.57–0.92 and $(U/La)_{PM}$=0.45–0.80. Except that the 01DB-152 sample could be attributed to significant crustal assimilation en route, others generally show decreasing of $^{87}Sr/^{86}Sr(t)$ ratio and increasing of $\varepsilon_{Nd}(t)$ value with the increase of SiO_2 (Fig. 8b–c). This is on contrary with the patterns that might be caused by crustal assimilation or assimilated fractionation crystallization (AFC) process (DePaolo, 1981). There is also a lack of the trend where $\varepsilon_{Nd}(t)$ values decrease with the increase of *mg*-number (Fig. 8d). These evidences, together with constant K_2O/TiO_2 ratio for these rocks, clearly argue against an AFC process. Therefore the variability of elemental and isotopic compositions for

Table 4
Pb isotopic data of early Cretaceous mafic dikes from the NDC and contemporaneous basaltic-andesitic rocks from the NHY

Sample	$^{238}U/^{204}Pb$	$^{232}Th/^{204}Pb$	$^{206}Pb/^{204}Pb$	$^{207}Pb/^{204}Pb$	$^{208}Pb/^{204}Pb$	$(^{206}Pb/^{204}Pb)i$	$(^{207}Pb/^{204}Pb)i$	$(^{208}Pb/^{204}Pb)i$	Δ7/4	Δ8/4
Mafic dikes from the NDC (~129 Ma)										
01DB-97	5.566	31.366	16.818	15.365	37.821	16.705	15.359	37.618	5.7	179.5
20BHY-81	3.997	23.241	16.485	15.314	37.353	16.404	15.310	37.203	4.1	174.4
20BHY-84	3.995	23.225	16.487	15.311	37.304	16.406	15.307	37.154	3.8	169.2
20BHY-86	4.224	23.795	16.454	15.337	37.267	16.368	15.333	37.113	6.7	169.8
01DB-106	6.910	40.898	17.119	15.417	38.179	16.978	15.410	37.916	7.9	176.2
01DB-134	3.569	13.963	16.045	15.274	36.793	15.972	15.271	36.703	4.8	176.5
01DB-136	4.505	14.722	15.998	15.261	36.707	15.906	15.256	36.612	4.1	175.4
01DB-152	3.890	15.071	16.672	15.350	37.251	16.593	15.346	37.154	5.6	146.7
01DB-162	6.211	31.665	16.648	15.370	37.416	16.521	15.364	37.212	8.2	161.1
Basaltic-andesitic rocks from the NHY (135–116 Ma)										
99XT-1	3.402	28.257	16.973	15.366	37.895	16.904	15.363	37.712	4.0	164.8
99XT-2	2.954	23.369	17.014	15.364	37.863	16.953	15.361	37.712	3.2	158.9
99XT-3	2.829	23.626	16.895	15.376	37.696	16.838	15.373	37.543	5.7	156.0
99XT-4	2.737	24.095	16.484	15.328	37.346	16.428	15.325	37.190	5.3	170.1
99XT-11	4.004	23.281	16.508	15.348	37.418	16.426	15.344	37.267	7.2	178.1
99XT-15	2.799	23.376	16.499	15.328	37.387	16.442	15.325	37.236	5.2	173.1
20BHY-14	2.778	24.453	16.967	15.369	37.869	16.910	15.366	37.711	4.2	164.0

$\lambda_{U238}=1.55125\times10^{-10}$ /year, $\lambda_{U235}=9.848\times10^{-10}$ /year, $\lambda_{Th232}=4.9475\times10^{-11}$ /year (Steiger and Jäger, 1977). Initial Pb isotopic ratios were calculated using the measured whole-rock Pb isotopic compositions, whole-rock U, Th and Pb contents (ICP-MS) by assuming 130 Ma for early Cretaceous mafic dikes from the NDC and contemporaneous basaltic-andesitic rocks from the NHY. $\Delta7/4=((^{207}Pb/^{204}Pb)_i-(^{207}Pb/^{204}Pb)_{NHRL})\times100$; $\Delta8/4=((^{208}Pb/^{204}Pb)_i-(^{208}Pb/^{204}Pb)_{NHRL})\times100$; $(^{207}Pb/^{204}Pb)_{NHRL}=0.1084\times(^{206}Pb/^{204}Pb)_i+13.491$ (Hart, 1984); $(^{208}Pb/^{204}Pb)_{NHRL}=1.209\times(^{206}Pb/^{204}Pb)_i+15.627$ (Hart, 1984).

the rocks from both tectonic units more likely indicates the involvement of crustal components in magma source region rather than crustal assimilation en route through the crust.

As discussed above, these samples have $mg=0.41$–0.65, Cr = 11–299 ppm and Ni = 25–100 ppm. Such characteristics suggest that they might have undergone certain degrees of crystal fractionation from parental magmas. The correlation between CaO/Al_2O_3 and MgO (Fig. 3h) and the pattern of decreasing Ni and Cr contents with decreasing MgO (Fig. 3i–j) support fractionation of olivine and clinopyroxene. Slightly negative Eu anomaly (Eu/Eu* = 0.68–0.90) and negative Sr anomaly in the spider diagram for some samples may be attributed to fractionation of plagioclase. Depletion in Ti and negative correlation between P_2O_5, TiO_2 and SiO_2 (Fig. 3f–g) are likely related to Fe–Ti oxides and apatite fractionation. Therefore, the geochemical signatures above suggest that these magmas likely encountered a certain extent of olivine + clinopyroxene ± Fe–Ti oxides ± apatite ± plagioclase differentiation.

5.2. Source characteristics

The LILEs and LREE enrichment and HFSEs depletion suggest that the mantle source of these rocks has compositional similarity with mantle wedge (Stern, 2002). High La/Nb (2.1–4.8), Ba/Nb (41–189) and Zr/Nb ratios (12.0–22.8) in these rocks are clearly distinctive to the features for most intraplate volcanic rocks (La/Nb = 0.5–2.5 and Ba/Nb = 1–20), but similar to arc volcanics worldwide (Fig. 9). In the plots of Pb isotopic ratios (Fig. 6a–b), these rocks define a trend toward the field of Smoky Butte lamprorites with very low $(^{206}Pb/^{204}Pb)_i$ ratios, which are representative of an origin from a highly metasomatised lithospheric mantle (Fraser et al., 1985). Recent studies on the Taihangshan lamprophyres (Chen and Zhai, 2003) and Jinan gabbros (Guo et al., 2001; Zhang et al., 2004) show that late Mesozoic lithospheric mantle beneath the Central NCC has an EMI-like isotopic character. The basaltic rock from the NCC exterior (i.e., the Jiaodong and Fangcheng areas), which are derived from the lithospheric mantle

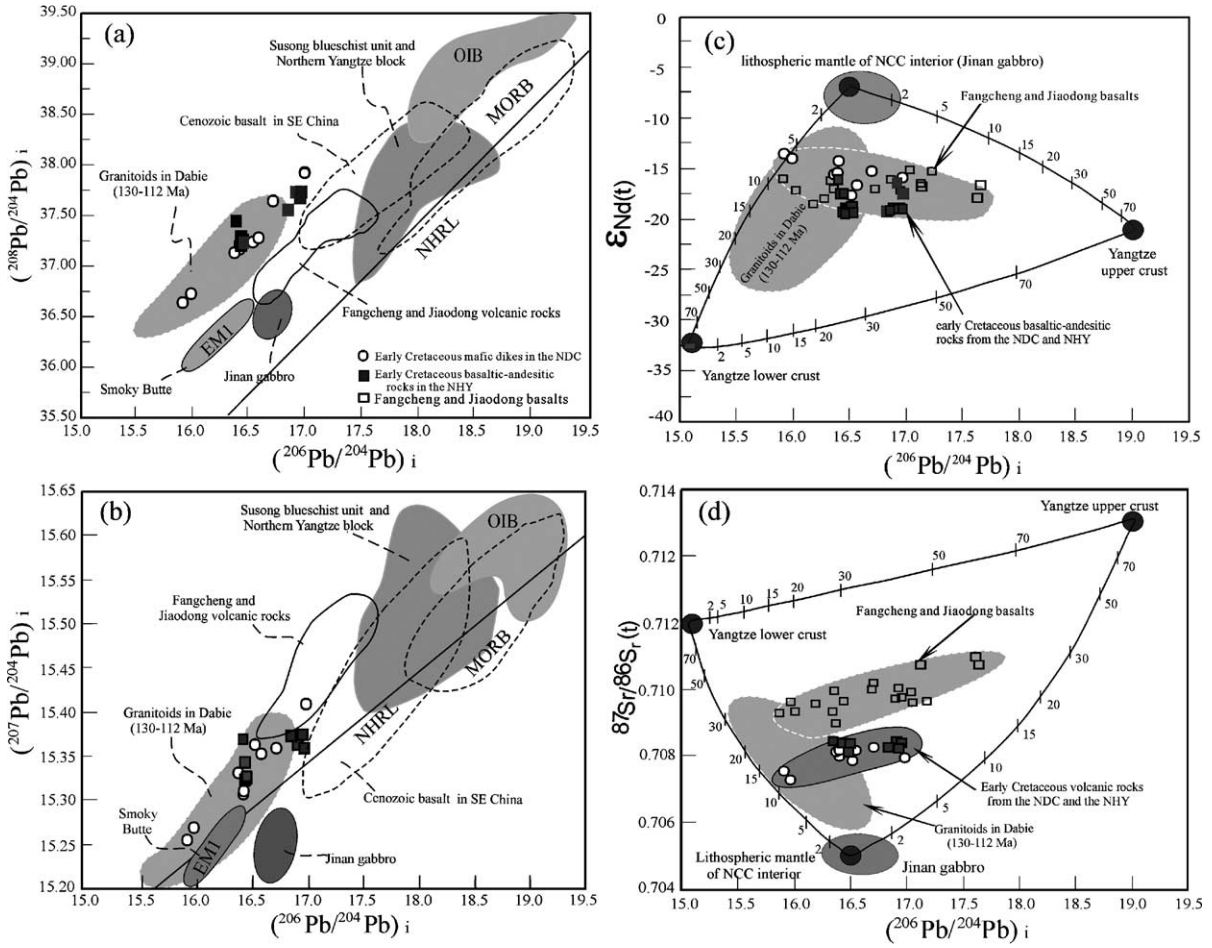

Fig. 6. Initial $^{206}Pb/^{204}Pb$ versus $^{207}Pb/^{204}Pb$ (a), $^{208}Pb/^{204}Pb$ (b), $^{87}Sr/^{86}Sr(t)$ (c) and $\varepsilon_{Nd}(t)$ (d) diagrams for early Cretaceous mafic dikes from the NDC and contemporaneous basaltic-andesitic rocks from the NHY, in comparison with Fangcheng basalts and mafic rocks from Jiaodong (Yang, 2000; Zhang et al., 2002a,b; Qiu et al., 2002) and Cretaceous granitoids in the Dabie Orogen (Zhang et al., 2002a,b). Fields for MORB, OIB and NHRL (north hemisphere reference line) are taken from Hart (1984), and Smoky Butte lamproites from Fraser et al. (1985). Cenozoic basalts in SE China are from Zou et al. (2000). Field of Jinan gabbros is from Zhang et al. (2004), and Mesozoic mafic rocks from Susong blueschist unit and the northern Yangtze block are from Kuang and Zhang (2002) and Yan et al. (2003). The calculation parameters of Pb (ppm) and $^{206}Pb/^{204}Pb$ in (c–d) are 3.5 and 16.50 for the NCC lithospheric mantle, 25 and 15.10 for the Yangtze lower crust, and 30 and 19.00 for the Yangtze upper/middle crust, respectively (Zhang et al., 1994, 1999, 2002a,b, 2004; Li and Yan, 2003). The results show that mafic rocks in the Dabie Orogen can be interpreted as derivation of the NCC lithospheric mantle hybridized by the Yangtze lower and upper/middle crustal materials.

highly modified by the subduction processes (Yang, 2000; Fan et al., 2001; Zhang et al., 2002a,b; Zhang and Sun, 2002), are characterized by high LILE enrichment, HFSE depletion, higher $^{87}Sr/^{86}Sr(t)$ and $(^{208}Pb/^{204}Pb)_i$ ratios and lower $\varepsilon_{Nd}(t)$ values (Figs. 4–6), similar to those for the rocks from both tectonic units. Thus the geochemical signatures above suggest that these rocks originated from subduction-modified lithospheric mantle. The systematic studies of stable isotopes on rocks from the Dabie Orogen reveals that both subduction and exhumation were rapid, analogous to an ice cream-frying model, with a short residence time of the subducted slab at mantle depths, and that the flux of slab fluid was of low volume during plate subduction and prograde metamorphism (Zheng et al., 2003). The general absence of syncolli-

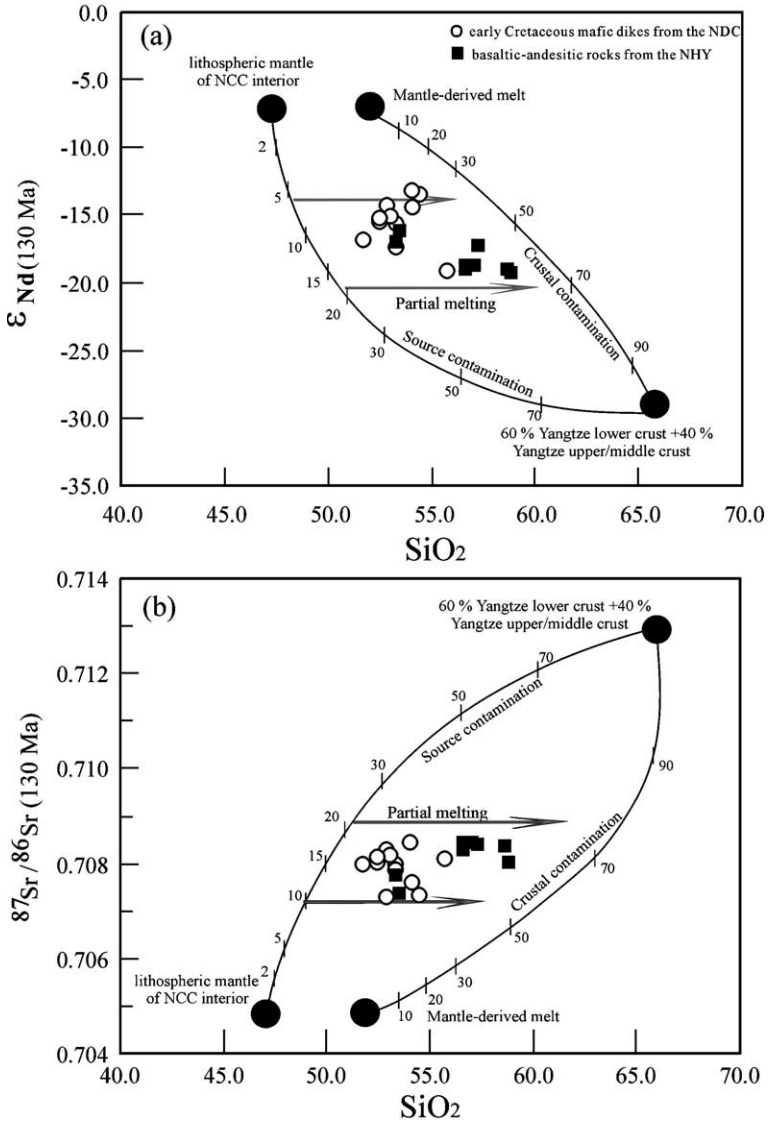

Fig. 7. Plots of SiO_2 versus $^{87}Sr/^{86}Sr$(130 Ma) (a) and ε_{Nd} (130 Ma) (b). The numbers indicate the percentages of participation of the crustal components. The end member of an enriched lithospheric source is resemble to that beneath the Central NCC (SiO_2=47 wt.%, Nd=4 ppm, Sr=60 ppm, $^{87}Sr/^{86}Sr(t)$=0.7050 and $\varepsilon_{Nd}(t)$=−7.0) and its derivation is comparable to Jinan gabbro with SiO_2=52 wt.%, Nd=45 ppm, Sr=800 ppm, $^{87}Sr/^{86}Sr(t)$=.7050 and $\varepsilon_{Nd}(t)$=−7.0. The end member of the Yangtze crustal materials is comprised by 40% Yangtze upper/middle crust (SiO_2=76 wt.%) and 60% Yangtze lower crust (SiO_2=59 wt.%). Other parameters are same in Fig. 5. The modeling results show that partial melting of the NCC lithospheric mantle contaminated by 10–20% Yangtze crustal components can account for the variation in SiO_2 and Sr–Nd isotopes for these coeval rocks from the NDC and NHY.

sional magmatism in the Dabie-Sulu orogen also supports insignificant flux of slab fluid into the overlying lithosphere during Triassic subduction/collision. Therefore it is most likely that the lithospheric mantle beneath the region was modified by the bulk digestion of subducted materials (Jahn et al., 1999; Fan et al., 2004) rather than by the metasomatism of subduction-related fluids.

Due to insignificant crustal assimilation during magma ascend, the Sr–Nd isotopic compositions

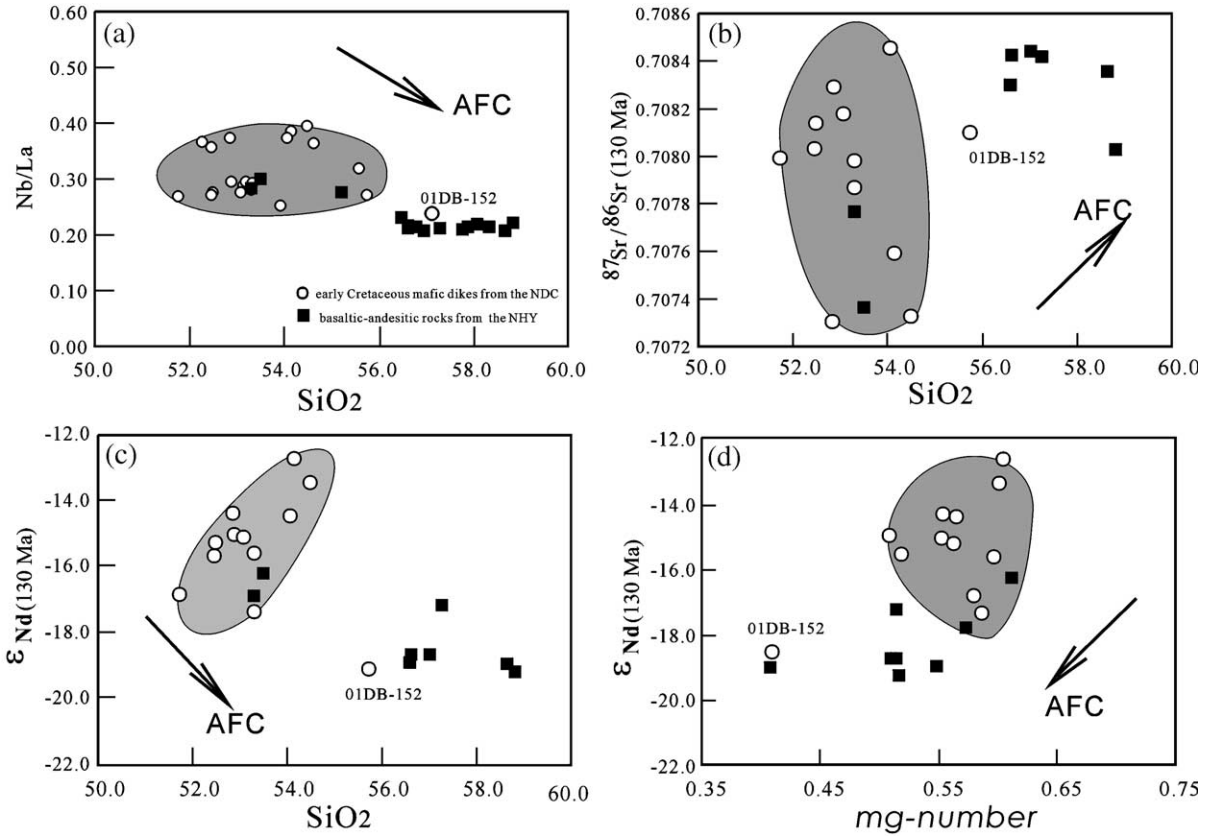

Fig. 8. Plots of SiO_2 versus Nb/La (a), $^{87}Sr/^{86}Sr(t)$ (b) and $\varepsilon_{Nd}(t)$ (c), and *mg*-number versus $\varepsilon_{Nd}(t)$ diagram (d) for the samples from the NDC and NHY.

shown on Fig. 5 might be interpreted as a derivation from a hybridized source. Three cases for the formation of the hybridized source can be proposed: (1) the NCC lithospheric mantle and NCC crust; (2) the Yangtze lithospheric mantle and Yangtze crust; and (3) the NCC lithospheric mantle and Yangtze crust. However, many workers (Hacker et al., 1998, 2000; Zheng et al., 2003; Ma et al., 1998; Zhang et al., 2002a,b) already emphasized the facts that the basement of the NDC and NHY has an affinity to the YB, and the Yangtze crust was northwardly subducted into the NCC mantle during Triassic (e.g., Okay et al., 1993; Xu et al., 2000; Mattauer et al., 1985; Cong, 1996; Fan et al., 2004; Jahn et al., 1999). Such considerations argue against the NCC crust and Yangtze lithospheric mantle as the possible end-member components for the hybridized source when accepting that the formation of the source was closely related to northward subduction of the YB. Therefore, the cases (1) and (2) are unlikely.

The basement and Paleozoic intrusive rocks from the North Qinling/Tongbei Mountains (with a tectonic affinity to the NCC) are characterized by highly radiogenic Pb isotopic ratios, whereas the South Qinling/Tongbei Mountains (with a tectonic affinity to the YB; see Zhang et al., 1994, 1996, 1999) are characterized by low radiogenic Pb isotopic ratios. The orthogneiss and amphibolites from the NDC, which are generally regarded as the representative of the Yangtze middle/lower crust (Ma et al., 2000), have $^{206}Pb/^{204}Pb = 15.81–17.24$ and $^{207}Pb/^{204}Pb = 15.16–15.46$ (Zhang et al., 2002a,b). Thus the low ^{206}Pb and ^{207}Pb relative to ^{204}Pb for the samples from both tectonic units should be related to the Yangtze lower crust (Li and Yan, 2003), and the Yangtze lower crust should be an important end-member component

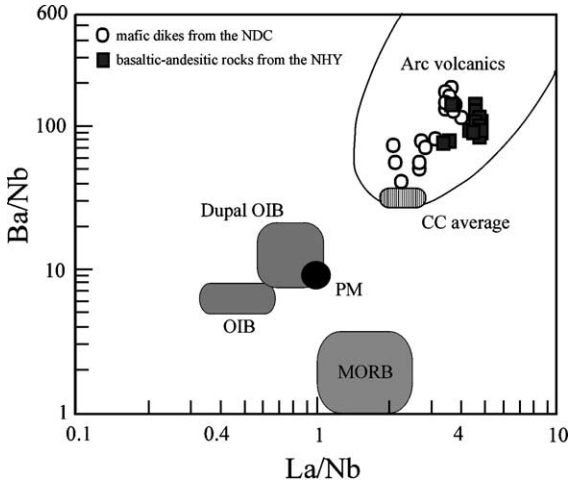

Fig. 9. Ba/Nb versus La/Nb plot showing that early Cretaceous mafic dikes from the NDC and contemporaneous basaltic-andesitic rocks from the NHY are characterized by high Ba/Nb and La/Nb ratios, falling into the field of arc volcanics. Data of PM and average continental crust are respectively from Sun and McDonough (1989), Taylor and McLennan (1985), and OIB, MORB from Le Roux (1986), and Dupal OIB from Jahn et al. (1999).

of the hybridized source. However, a simple mixing between the NCC lithospheric mantle and Yangtze lower crust should produce a positive correlation in the $^{206}Pb/^{204}Pb$-$\varepsilon_{Nd}(t)$ diagram, and a negative correlation in a $^{206}Pb/^{204}Pb$–$^{87}Sr/^{86}Sr(t)$ diagram (Zou et al., 2000). This is inconsistent with the generally reverse correlation patterns revealed for these rocks, which are away from the trends defined by the NCC lithospheric mantle and Yangtze lower crust (Fig. 6c–d). Thus a simple interpretation is that the correlations in Fig. 6c–d reflect the involvement of the upper/middle crustal components with high $^{206}Pb/^{204}Pb$, high $^{87}Sr/^{86}Sr(t)$ and slightly low $\varepsilon_{Nd}(t)$. The UHP rocks in the Dabie orogen (tectonically affiliating to the YB) have more radiogenic Pb isotopic compositions ($^{206}Pb/^{204}Pb = 17.2–19.9$ and $^{207}Pb/^{204}Pb = 15.3–15.7$) than those from the NDC, and are confined to shallower crustal level than grey gneisses (Ma et al., 2000; Zhang et al., 2002a,b). Zheng et al. (2003) suggested that the UHP rocks encountered meteoric-hydrothermal alteration at or near the earth's surface before subduction and UHP metamorphism. These observations indicate that the UHP rocks in the region can be regarded as the Yangtze middle/upper crustal components into melting source during subduction and exhumation. Therefore, the most likely scenario is that the source region for these rocks was a mixture of three components: NCC enriched lithospheric mantle, subducted Yangtze lower crust and Yangtze upper/middle crust.

To define the individual contribution of the three components in the mantle source for these rocks, a mixing calculation was performed based on Sr–Nd–Pb isotopic compositions. The results (Figs. 5 and 6c–d) show that the involvement of 5–15% Yangtze lower crust and 5–10% Yangtze upper/middle crust into the NCC lithospheric mantle can reasonably account for the Sr–Nd–Pb isotopic features for the rocks from both tectonic units. To further explore their chemical variations, assuming that the Yangtze upper/middle crust, Yangtze lower crust and NCC lithospheric mantle have $SiO_2 = 76$ wt.%, 59 wt.% and 47 wt.% (Fan et al., 2004), respectively, the subducted crustal materials are postulated to be equivalent to the mixture of 40% Yangtze upper/middle crust with 60% Yangtze lower crust on the basis of the aforementioned modeling results. These calculations show that the addition of 5–20% crustal materials into the NCC lithospheric mantle would not only suffice the observed Sr–Nd isotopic ratios but also have a range of ~49–52 wt.% in SiO_2 (Fig. 9a–b). Partial melting of such a hybridized source can explain the variations of major oxides for these rocks (Fig. 9a–b). Thus, we consider that these rocks from both tectonic units might be derived from a source region of the NCC lithospheric mantle contaminated by the deeply subducted Yangtze crustal materials.

5.3. Tectonic decoupling between surface suture and lithospheric boundary

There are two contrasting suggestions for the surface suture between the YB and NCC (Suo et al., 2000; Zhang et al., 2002a,b and reference therein). One suggests that the Wuhe-Shuihou fault represents the suture between the YB and NCC (Cong, 1996). The other advocates that the NDC is the subducted basement of the YB (Ames et al., 1996; Rowley et al., 1997; Ma et al., 1998; Okay et al., 1993) and the Xiaotian-Mozitan fault or the Liu'an-Hefei fault is the surface suture (Fig. 1b; Suo et al., 2000; Hacker et al., 2000). Recent studies support the later hypothesis (Li and Yan, 2003; Zhang et al., 2002a,b; Ma et al., 2000;

Kuang and Zhang, 2002; Hacker et al., 2000), based on: (1) The YB-related Paleozoic island-arc volcanics and the Neoprototerozoic tectonothermal event (~800 Ma; Hacker et al., 1998; Xue et al., 1997) exists in both tectonic units; and (2) the NDC also included a small quantity of Triassic HP-UHP rocks, which were interpreted as a part of the subducted Yangtze crust (Li and Yan, 2003; Xu et al., 2000). Thus, it is more likely that the crust of the NDC is tectonically affiliated to the YB, and the surface suture between the YB and NCC is located along the Xiaotian-Mozitan fault or other faults to the north.

The YB and NCC have distinctive crustal ages and tectonic histories (Gao et al., 1999; Qiu et al., 2000), suggesting that both blocks should have different lithospheric nature. Recent studies showed that Mesozoic mafic rocks from the Susong blueschist unit in the South Dabie (i.e., the Macheng area), northern YB (i.e., the Huangshi, Xinzhou areas and lower Yangtze River region) and YB interior (i.e. southern Hunan Province) generally have $^{87}Sr/^{86}Sr(i)<0.7067$, $\varepsilon_{Nd}(t)>-6$, $^{206}Pb/^{204}Pb>17.5$ (Wang et al., 2003b; Li et al., 2003; Yan et al., 2003), whereas Mesozoic mafic rocks in the Central NCC have $^{87}Sr/^{86}Sr(i)<0.7060$, $\varepsilon_{Nd}(t)=-6$ to -14, $^{206}Pb/^{204}Pb<17.3$ (Figs. 1a, 5 and 6; Li and Yan, 2003; Guo et al., 2001; Fan et al., 2001; Zhang et al., 2002a,b, 2004). These rocks from the NDC and NHY show similar elemental and Sr–Nd–Pb isotopic characteristics to those of the NCC exterior interpreted as origination of subduction-related lithospheric mantle. Such similarities suggest that these coeval rocks from both tectonic units share a similar mantle source region and geochemical affinity with those from the NCC.

Triassic deep subduction of the YB (Ames et al., 1996; Rowley et al., 1997; Ye et al., 2000; Zheng et al., 2001, 2003) most likely metasomatised the overlying lithospheric mantle by subduction-related fluid/melt or modified the overlying mantle by digestion of subducted materials (Fan et al., 2004; Jahn et al., 1999). As a result, the subduction-related lithospheric mantle and its derivation normally developed at the hanging wall rather than the footwall of the suture/lithospheric boundary (Jahn et al., 1999; Li and Yan, 2003; Wang et al., 2003a). If the lithospheric boundary between the YB and NCC was coupled with the surface suture (the Xiaotian-Mozitan fault or other faults to the north), the mafic magma derived from subduction-related lithospheric mantle should have only developed beneath the NHY to north rather than in the NDC to south of the Xiaotian-Mozitan fault. This notion is in contrast to the fact that subduction-related mafic magma extensively occurred at both the NHY and NDC. In combination with aforementioned discussion, we propose that early Cretaceous mafic rocks around the Wuhe-Shuihou fault that separates the NDC and SDC have a distinct affinity to the continental lithospheric mantles and tectonic histories. The spatial variations of geochemical signatures for early Cretaceous mafic rocks around the Wuhe-Shuihou fault suggest that the fault represents the Mesozoic lithospheric boundary between the YB and NCC despite the present-day surface suture is located at the Xiaotian-Mozitan fault or other faults to the north. That is, a case similar to eastern Carpathian Orogen (Andereescu and Demetrescu, 2001) and Himalaya-Tibet system (Chemenda et al., 2000). The tectonic decoupling between the surface suture and lithospheric boundary between the YB and NCC occurred before early Cretaceous (Li and Yan, 2003; Wang et al., 2003a). The Mesozoic lithospheric mantle beneath the NDC is tectonically affiliated with the NCC while its present-day crust has an affinity to the YB. Such a crustal detachment or tectonic decoupling is similar to that in the region east of the Tan-Lu fault (Li, 1994, 1995; Chung, 1999).

5.4. Possibly tectonic scenario of Dabie-Sulu Orogen

Fig. 10 summarizes the tectonic scenario of a subduction–collision–extension cycle for the Dabie Orogen. At 245–240 Ma, the Yangtze crust was deeply subducted into the NCC mantle along the Wuhe-Shuihou fault, accompanied by prograde metamorphism. Portions of subducted Yangtze crustal materials were contemporaneously trapped into the original lithospheric mantle (Fig. 10a). The rapid exhumation of the HP-UHP rocks then occurred at 230–210 Ma (Fig. 10b). The entire cycle of subduction, UHP prograde metamorphism and exhumation is analogous to an ice cream-frying model, and is estimated to take place at ~10–20 Ma (Zheng et al., 2001, 2003). During rapid exhumation, a part of the subducted crustal components was trapped into the overlying lithospheric mantle as structural lens, streak and pudding along the pre-existing fractures, although most were rapidly exhumed back to crustal level

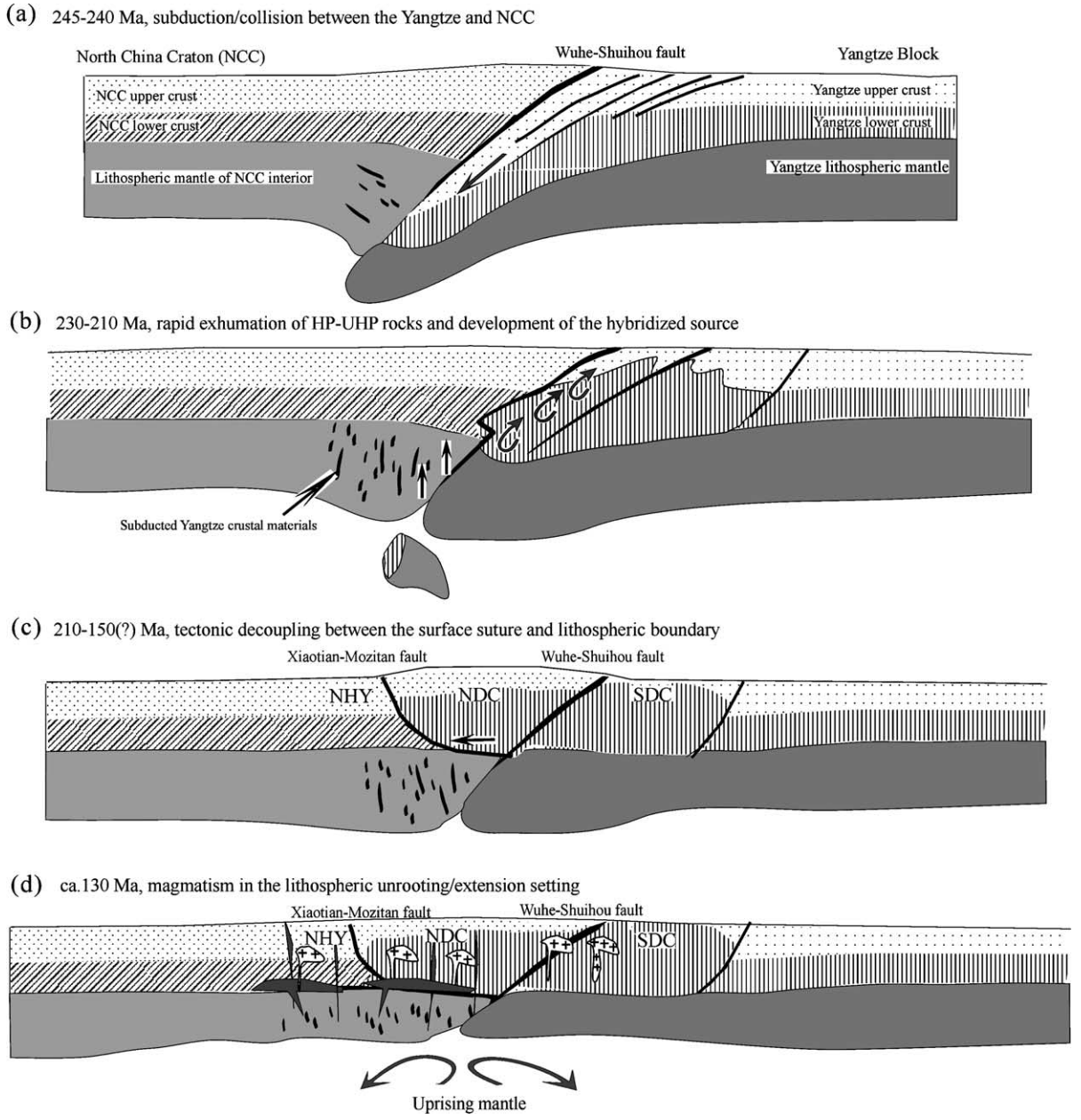

Fig. 10. Schematic cartoon illustrating the subduction/collision–exhumation–tectonic decoupling–extension of the Dabie Orogen. See text for detailed descriptions. In comparison with the cartoon proposed by Fan et al. (2004), the model considered that early Cretaceous mafic igneous rocks from the NDC originated from a similar heterogeneous mantle source modified by the subducted Yangtze crust with that of the NHY. However, it is especially emphasized in the model that the subducted Yangtze crust were trapped into original lithospheric mantle during not only slab subduction (245–240 Ma) but also the rapid exhumation of the HP-UHP rocks (230–210 Ma), and that the Yangtze crust was progressively thrust northward over the NCC to result in the development of tectonic decoupling between the lithospheric boundary and surface suture during 210–150 Ma.

(Fig. 10b; Hacker et al., 2000; Zheng et al., 2001, 2003; Fan et al., 2004). As a result, the hybridized source developed. Fan et al. (2004) and Faure et al. (1999) also concluded that voluminous subducted crust could be settled in the overlying lithospheric mantle during deeply subduction and subsequent exhumation of the HP-UHP rocks in response to buoyancy from the convective mantle (Anderson et al., 1991). During 210–150(?) Ma, the Yangtze crust was progressively thrusted northward over the NCC (Liu and Wang, 1999; Guo et al., 2002), which resulted in the development of the crustal detachment and tectonic decoupling between the lithospheric boundary and surface suture (Fig. 10c). At ~130 Ma, lithospheric extension predominantly developed in response to the rapidly lithospheric unrooting and further exhumation of the HP-UHP rocks. The extension results in the melting of the hybridized source to generate these rocks of the NDC and NHY (Fig. 10d).

Several different scenarios have been proposed for the Triassic collision style between the YB and NCC, such as, northward subduction/collision along the suture of a subparallel lineation in the Subei basin (Chung, 1999), or a clockwise collision along the Yanji-Imjingang-Sulu-Tanlu zone (Zhang, 1997; Gilder et al., 1999). The Mesozoic mafic rocks from Jiaodong, Fangcheng, Mengyin, the NDC and NHY shown on Fig. 1a share similar elemental and Sr–Nd–Pb isotopic compositions, and can be interpreted as the melting product of subduction-related lithospheric mantle (Fan et al., 2001, 2004; Qiu et al., 2002; Wang et al., 2002; Li and Yan, 2003; Jahn et al., 1999; Zhang et al., 2002a,b; Yang, 2000). They predominantly occurred in the northwest of the Sulu-Tanlu-Wuhe-Shuihou zone (Fig. 1a). It is notable that the Paleozoic passive continental margin sedimentary basins and late Triassic–early Jurassic foreland molasse basins are dominantly NE-trending in the lower Yangtze River region east of the Tan-Lu fault (Yin and Nie, 1993; Zhang, 1997), whereas late Triassic–middle Jurassic sedimentary basins (i.e., Jianghan and Hefei basins) display a roughly EW-trending orientation in region west of the Tan-Lu fault. This appears to support the clockwise collision of the YB along the Sulu-Tanlu-Wuhe-Shuihou zone relative to the NCC (see insert of Fig. 1a; Zhang, 1997; Gilder et al., 1999). That is to say, the Triassic collision of the YB and NCC is probably characterized by clockwise contact firstly along the NE-trending Sulu-Tanlu zone and then the roughly E–W trending Wuhe-Shuihou fault (Zhang, 1997; Gilder et al., 1999).

6. Concluding remarks

The mafic dikes from the NDC intruded at 127.6–131.8 Ma ($^{40}Ar/^{39}Ar$ plateau ages), and the basaltic-andesitic rocks of the NHY erupted at 135–116 Ma. These coeval rocks have similar geochemical characteristics, i.e. enrichment of LILEs, depletion of HFSEs, very low $\varepsilon_{Nd}(t)$ value (−12.7 to −19.2), $^{206}Pb/^{204}Pb$ (15.97–16.98), and prominent positive Δ8/4 (146.7–179.5) and Δ7/4 (3.2–8.2). Such geochemical signatures are interpreted as the product of subduction-related lithospheric mantle source, tectonically similar to that beneath the NCC exterior, contaminated by the subducted Yangtze crust. The spatial variations of the geochemical signatures for early Cretaceous basic-intermediatic rocks around the Wuhe-Shuihou fault that separated the NDC and SDC supports an early Mesozoic tectonic decoupling model in the Dabie Orogen. The Wuhe-Shuihou fault likely represents the Mesozoic lithospheric boundary between the YB and NCC, despite the present-day surface suture is located along the Xiaotian-Mozitan fault or other faults to the north.

Acknowledgements

We would like to thank Mr. L. Qi for his help in ICP-MS performance and Mr. R.-H. Zhang for Sr–Nd isotope analysis. We are grateful to James Z., Profs. Y.-H. Zhang, Y.-G. Xu and J.-F. Chen for their reading of the manuscript and helpful discussions and suggestions. Profs. S.-L. Chung, R.-L. Rudnick and an anonymous reviewer are thanked for their critical and constructive review, which led to major improvement of the manuscript. This study was financially supported by the National Nature Sciences Foundation of China (grant nos. 40334039, 40421303, and 49873011), the Ministry of Science and Technology of China (G1999075504) and Chinese Academy of Sciences (GIGCX-03-01; KZCX2-102). **[RLR]**

References

Ames, L., Zhou, G., Xiong, B., 1996. Geochronology and isotopic character of high-pressure metamorphism with implications for collision of the Sino-Korean and Yangtze cratons, Central China. Tectonics 15, 472–489.

Andereescu, M., Demetrescu, C., 2001. Rheological implications of the thermal structure of the lithosphere in the convergence zone of the Eastern Carpathians. J. Geodyn. 31, 373–391.

Anderson, T.B., Jamtveit, B., Dewey, J.F., Swensson, E., 1991. Subduction and eduction of continental crust: major mechanism during continental–continental collision and orogenic extensional collapse, a model based in the south Norwegian Caledonides. Terra Nova 3, 301–310.

Chemenda, A.I., Burg, J.P., Mattauer, M., 2000. Evolutionary model of the Himalaya-Tibet system: geopoem based on new modeling, geological and geophysical data. Earth Planet. Sci. Lett. 174, 397–409.

Chen, J.F., Jahn, B.M., 1998. Crustal evolution of southeastern China: Nd and Sr isotopic evidence. Tectonophysics 284, 101–133.

Chen, B., Zhai, M.G., 2003. Geochemistry Of Late Mesozoic Lamprophyre dikes from the Taihang Mountains, North China and implications for the subcontinental lithospheric mantle. Geol. Mag. 140 (1), 87–93.

Chen, C.H., Lo, C.H., Teng, L.S., 1995. Preliminary geochemical result of the basic plutons and basic-intermediate dikes from northern Dabieshan area, China. Taipei: extended abstracts of the conference on geology across the Taiwan strait, pp. 4–7.

Chen, B., Jahn, B.M., Wei, C.J., 2002. Petrogenesis of Mesozoic granitoids in the Dabie UHP complex, central china: trace element and Nd–Sr isotopic evidence. Lithos 60, 67–88.

Chung, S.L., 1999. Trace element and isotope characteristics of Cenozoic basalts around the Tanlu Fault with implications for the eastern plate boundary between North and South China. J. Geol. 107, 301–312.

Cong, B.L., 1996. Ultrahigh-pressure metamorphic rocks in the Dabie-Sulu region of China: Science Press, Beijing, China and Kluwer Acad Publ Dordrecht 1–224.

DePaolo, D.J., 1981. Trace element and isotopic effects of combined wall rock assimilation and fractional crystallization. Earth. Planet. Sci. Lett. 53, 189–202.

Fan, W.M., Guo, F., Wang, Y.J., 2001. Post-orogenic bimodal volcanism along the Sulu Orogenic belt in eastern China. Phys. Chem. Earth, Part A Solid Earth Geod. 26 (9–10), 733–746.

Fan, W.M., Guo, F., Wang, Y.J., Zhang, M., 2004. Late Mesozoic volcanism in the northern Huaiyang tectono-magmatic belt, central China: partial melts from a lithospheric mantle with subducted continental crust relicts beneath the Dabie Orogen? Chem. Geol. 209 (1–2), 27–48.

Faure, M., Lin, W., Shu, L.S., Sun, Y., Scharer, U., 1999. Tectonics of the Dabieshan (eastern China) and possible exhumation mechanism of ultra high-pressure rocks. Terra Nova 11, 251–258.

Fraser, K.J., Hawkesworth, C.J., Erland, A.J., Mitchell, R.H., Scott-Smith, B.H., 1985. Sr–Nd–Pb isotopic and minor element geochemistry of lamproites and kimberlites. Earth. Planet. Sci. Lett. 76, 5–20.

Gao, S., Lin, W.L., Qiu, Y.M., 1999. Contrasting geochemical and Sm–Nd isotopic compositions of Archaean metasediments from the Kongling high-grade terrain of the Yangtze craton: evidence for cratonic evolution and redistribution of REE during crustal anatexis. Geochim. Cosmochim. Acta 63 (13/14), 2071–2088.

Gilder, S.A., Leloup, P.H., Courtillot, V., Yan, C., Coe, R.S., Zhao, X.X., et al., 1999. Tectonic evolution of the Tancheng-Lujiang (Tan-Lu) fault via Middle Triassic to early Cenozoic paleomagnetic data. J. Geophys. Res. 104 (B7), 15365–15390.

Guo, F., Fan, W.M., Wang, Y.J., 2001. Late-Mesozoic mafic intrusive complexes in north china block: constraints on the nature of subcontinental lithospheric mantle. Phys. Chem. Earth, Part A Solid Earth Geod. 26 (9–10), 759–771.

Guo, H., Wu, Z.W., Cai, Y.C., Hong, M., 2002. Mesozoic overthrust nappe tectonic system in the Dabieshan orogenic belt. Geoscience 16 (2), 121–129 (in Chinese with English abstract).

Hacker, B.R., Ratschbacher, L.W., Ireland, L., 1998. U/Pb zircon ages constrain the architecture of the ultrahigh-pressure Qinling-Dabie Orogen, China. Earth Planet. Sci. Lett. 161, 215–230.

Hacker, B.R., Ratschbacher, L., Webb, L., 2000. Exhumation of ultrahigh-pressure continental crust in east central China: late Triassic–early Jurassic tectonic unroofing. J. Geophys. Res. 105 (B6), 13339–13364.

Hart, S.R., 1984. A large-scale isotopic anomaly in the Southern Hemisphere mantle. Nature 309, 753–757.

Jahn, B.M., Wu, F.Y., Lo, C.H., 1999. Crust–mantle interaction induced by deep subduction of the continental crust: geochemical and Sr–Nd isotopic evidence from post-collisional mafic–ultramafic intrusions of the northern Dabie Complex, Central China. Chem. Geol. 157, 119–146.

Kuang, S.P., Zhang, B.R., 2002. Tectonic subdivision of Dabie orogenic belt, central china: evidence from Pb isotope geochemistry of late Mesozoic basalts. Chin. J. Geochem. 21 (2), 147–155.

Le Roux, A.P., 1986. Geochemical correlation between southern African kimberlites and south Atlantic hotspots. Nature 324, 243–245.

Li, Z.X., 1994. Collision between the North and South China Blocks: a crustal-detachment model for suturing in the region east of the Tanlu Fault. Geology 22, 739–742.

Li, S.G., Yan, W., 2003. Decoupling of surface and subsurface sutures in the Dabie Orogen and a continent–collisional lithospheric-wedging model: Sr–Nd–Pb isotopic evidences of Mesozoic igneous rocks in eastern China. Chin. Sci. Bull. 48 (8), 831–838.

Li, S.G., Xiao, Y.L., Liou, D.L., 1993. Collision of the North China and Yangtze blocks and formation of coesite-bearing eclogites: timing and process. Chem. Geol. 109, 89–111.

Li, X.H., Chung, S.L., Zhou, H.W., Lo, C.H., Liu, Y., Chen, C.H., 2003. Jurassic intraplate magmatism in Southern Hunan-Eastern Guangxi: $^{40}Ar/^{39}Ar$ dating, geochemistry, Sr–Nd isotopes and implications for tectonic evolution of South China. In: Malpas, J., Fletcher, C.J., Aitchison, J.C., Ali, J. (Eds.), Aspects of the Tectonic Evolution of China, Special Publications, vol. 226. Geological Society, London, pp. 193–216.

Lin, S.F., 1995. Collision between the North and South China blocks: a crustal-detachment model for suturing in the region east of the Tanlu fault. Geology 23, 574–575.

Liu, W.C., Wang, G.S., 1999. Mesozoic thrust and nappe tectonics in northern Huaiyang region. Geoscience 13 (2), 143–149 (in Chinese with English abstract).

Ma, C.Q., Li, Z.C., Ehlers, C., 1998. A post-collisional magmatic plumbing system: Mesozoic granitoid plutons from the Dabieshan high-pressure and ultrahigh-pressure metamorphic zone, East-central China. Lithos 45, 431–456.

Ma, C.Q., Ehlers, C., Xu, C.H., 2000. The roots of the Dabieshan ultrahigh-pressure metamorphic terrain: constraints from geochemistry and Nd–Sr isotope systematics. Precambrian Res. 102, 279–301.

Mattauer, M., Matte, P., Malavieille, J., Tapponnier, P., Maluski, H., Xu, Z.Q., et al., 1985. Tectonics of the Qinling belt: build-up and evolution of eastern Asia. Nature 317, 496–500.

Middlemost, E.A.K., 1994. Naming materials in the magma/igneous rock system. Earth Sci. Rev. 37, 15–224.

Okay, A.I., Sengor, A.M.C., Satir, M., 1993. Tectonics of an ultrahigh-pressure metamorphic terrain: the Dabie Shan/Tongbie Shan Orogen, China. Tectonics 12, 1320–1334.

Potts, P.J., Thompson, M., Kanes, J.S., Wilson, S., 2000. GeoPT6. an international proficiency test for analytical geochemistry laboratories, report on round 6 (OU-3, Nanhoron Microgranite).

Qi, L., Hu, J., Greggoire, C., 2000. Determination of trace elements in granites by inductively coupled plasma mass spectrometry. Talanta 51, 507–513.

Qiu, Y.M., Gao, S., McNaughton, N.J., Groves, D.I., Ling, W.L., 2000. First evidence of > 3.2Ga continental crust in the Yangtze craton of South China and its implications for Archaean crustal evolution and Phanerozoic tectonics. Geology 28 (1), 11–14.

Qiu, J.S., Xu, X.S., Lo, Q.H., 2002. Potassium-rich volcanic rocks and lamprophyres in western Shandong Province: $^{40}Ar/^{39}Ar$ dating and source tracing. Chin. Sci. Bull. 4 (2), 91–99.

Rowley, D.B., Xue, F., Tucker, R.D., 1997. Ages of ultrahigh pressure metamorphism and protolith orthogneisses from the eastern Dabie shan: U/Pb zircon geochronology. Earth Planet. Sci. Lett. 151, 191–203.

Sang, H.Q., Wang, S.S., Qiu, J., 1996. The $^{40}Ar–^{39}Ar$ ages of pyroxene, hornblende and plagioclase in Taipingzhai granulites in Qianxi County, Hebei Province and their geological implications. Acta Petrologica Sin. 12 (4), 390–400 (in Chinese with English abstract).

Steiger, R.H., Jäger, E., 1977. Subcommission on geochronology; convection on the use of decay constants in geochronology and cosmochronology. Earth Planet. Sci. Lett. 36, 359–362.

Stern, R.J., 2002. Subduction zones. Rev. Geophys. 40 (4), 1–38.

Sun, S.S., McDonough, W.F., 1989. Chemical and isotopic systematics of oceanic basalts: implication for mantle composition and processes. In: Sauders, A.D., Norry, M.J. (Eds.), Magmatism in the Ocean Basins, Special Publication, vol. 42. Geological Society, London, pp. 313–345.

Suo, S.T., Zhong, Z.Q., You, Z.D., 2000. Location of Triassic tectonic suture line between collided Sino-Korean and Yangtze cratons in Dabie-Sulu tectonic zone. Earth Sci. 25 (2), 111–116.

Taylor, S.R., McLennan, S.M., 1985. The Continental Crust: Its Composition and Evolution. Oxford Press, Blackwell, pp. 312.

Thompson, M., Potts, P.J., Kanes, J.S., Wilson, S., 2000. GeoPT5. an international proficiency test for analytical geochemistry laboratories, report on round 5 (August 1999). J. Geostand. Geoanal. 24 (1), 137.

Tsai, C.H., Liou, J.G., 2000. Eclogite-facies relics and inferred ultra high-pressure metamorphism in the North Dabie Complex, central-eastern China. Am. Mineral. 5, 1–8.

Wang, Y.J., Fan, W.M., Guo, F., 2002. K–Ar dating of late Mesozoic volcanism and geochemistry of volcanic gravels in the North Huaiyang belt, Dabie Orogen: constrains on the stratigraphic framework and exhumation of the northern dabie orthogneiss complex. Chin. Sci. Bull. 47, 1668–1695.

Wang, Y.J., Fan, W.M., Guo, F., Peng, T.P., 2003a. Geochemical Characteristics of late Mesozoic volcanic rocks in the hinterland of North Dabie terrene and their implications. Front. Geosci. 10 (4), 529–530.

Wang, Y.J., Fan, W.M., Guo, F., Peng, T.P., 2003b. Geochemistry of Mesozoic mafic rocks around the Chenzhou-Linwu fault in South China: implication for the lithospheric boundary between the Yangtze and the Cathaysia blocks. Int. Geol. Rev. 45 (4), 267–288.

Wu, X.Y., Xu, Y.G., Ma, J.L., Xu, J.F., Wang, Q., 2003b. Geochemistry and petrogenesis of the Mesozoic high-mg diorites from western Shandong. Geotecton. Metallogen. 3 (in Chinese with English abstract).

Xu, Y.G., 2002. Evidence for crustal components in the mantle and constraints on crustal recycling mechanisms: pyroxenite xenoliths from Hannuoba, North China. Chem. Geol. 182, 301–322.

Xu, S.T., Liu, Y.C., Su, W., 2000. Discovery of the eclogite and its petrography in the northern Dabie Mountains. Chin. Sci. Bull. 49 (3), 273–278.

Xue, F., Rowley, D.B., Tucke, R.D., 1997. U–Pb zircon ages of granitoid rocks in the North Dabie complex, eastern Dabieshan, China. J. Geol. 105, 744–753.

Yan, J., Chen, J.F., Yu, G., Qian, H., Zhou, T.X., 2003. Pb isotopic characteristics of late Mesozoic mafic rocks from the lower Yangtze region: evidence for enriched mantle. Geol. J. China Univ. 9 (2), 195–206.

Yang, J.H., 2000. Age and metallogenesis of gold mineralization in Jiaodong Peninsula, eastern China: constraints on the interaction of mantle/crust and metallogenesis/lithospheric evolution. Unpubl PhD thesis, Institute of Geology and Geophysics. Chinese Academy of Sciences (in Chinese).

Ye, K., Ye, D.N., Cong, B.L., 2000. The possible subduction of continental material to depths greater than 200 km. Nature 407, 734–736.

Yin, A., Nie, S., 1993. An indentation model for the North and South China collision and the development of the Tan-Lu and Honan fault systems, eastern Asia. Tectonics 12, 801–813.

Zhang, K.J., 1997. North and South China collision along the eastern and southern North China margins. Tectonophysics 270, 145–156.

Zhang, H.F., Sun, M., 2002. Geochemistry of Mesozoic basalts and mafic dikes in southeastern North China craton, and tectonic implication. Int. Geol. Rev. 44, 370–382.

Zhang, B.R., Luo, T.C., Gao, S., Ouyang, J.P., Chen, D.X., Ma, Z.D., et al., 1994. Geochemical Study of the Lithosphere, Tectonism and Metallogenesis in the Qinling-Dabashan Region. Press of China University Of Geosciences, Wuhan, pp. 1–446.

Zhang, H.F., Zhang, B.R., Zhao, Z., Luo, T., 1996. Continental crust subduction and collision along Shangdan tectonic belt of east Qinling: evidence from Pb, Nd and Sr isotopes of granitoids. Sci. China, Ser. D: Earth Sci. 39, 273–282.

Zhang, H.F., Zhang, L., Gao, S., Zhang, B.R., Wang, L.S., 1999. Pb isotopic compositions of metamorphic rocks and intrusive rocks in Tongbai region and their geological implication. Earth Sci. 24 (3), 223–269 (in Chinese with English abstract).

Zhang, Hong-Fei, Gao, S., Zhong, Z.Q., Zhang, B.R., Zhang, L., Hu, S.H., 2002. Geochemical and Sr–Nd–Pb isotopic compositions of Cretaceous granitoids: constrains on tectonic framework and crustal structure of the Dabieshan ultrahigh-pressure metamorphic belt, China. Chem. Geol. 186, 281–299.

Zhang, Hong-Fu, Sun, M., Zhou, X.H., Fan, W.M., Zhai, M.G., Yin, J.F., 2002a. Mesozoic lithospheric destruction beneath the north china craton: evidence from major-, trace-element and Sr–Nd–Pb isotope studies of Fangcheng basalts. Contrib. Mineral. Petrol. 144, 241–253.

Zhang, H.F., Sun, M., Zhou, M.F., Fan, W.M., Zhou, X.H., Zhai, M.G., 2004b. Highly heterogeneous late Mesozoic lithospheric mantle beneath the North China Craton: evidence from Sr–Nd–Pb isotopic systematics of mantle igneous rocks. Geol. Mag. 141, 55–62.

Zheng, Y.F., Fu, B., Li, Y.L., 2001. Oxygen isotope composition of granulites from Dabieshan in eastern China and its implications for geodynamics of Yangtze plate subduction. Phys. Chem. Earth, Part A Solid Earth Geod. 26 (9–10), 673–684.

Zheng, Y.F., Fu, B., Gong, B., Li, L., 2003. Stable isotope geochemistry of ultrahigh pressure metamorphic rocks from the Dabie-Sulu orogen in China: implications for geodynamics and fluid regime. Earth-Sci. Rev. 62, 105–161.

Zou, H.B., Zindler, A., Xu, X.S., 2000. Major, trace element, and Nd, Sr and Pb studies of Cenozoic basalts in SE China: mantle sources, regional variations, and tectonic significance. Chem. Geol. 171, 33–47.